Mitochondrial Energy Transformation Capacity Influences Brain Activation During Sensory, Affective, and Cognitive Tasks

Ke Bo[1*]
Catherine Kelly[2]
Caroline Trumpff[2]
Michio Hirano[3]
Michel Thiebaut de Schotten[5,6]
Martin Picard[2,3,4*]
Tor D. Wager[1*]

1 Department of Psychological and Brain Sciences, Dartmouth college, Hanover, NH

2 Department of Psychiatry, Division of Behavioral Medicine, Columbia University Irving Medical Center, New York, USA

3 Department of Neurology, H. Houston Merritt Center for Neuromuscular and Mitochondrial Disorders, Columbia University Translational Neuroscience Initiative, Columbia University Irving Medical Center, New York, USA

4 Robert N Butler Columbia Aging Center, Columbia University Mailman School of Public Health, New York, NY, USA

5 Groupe d'Imagerie Neurofonctionnelle, Institut des Maladies Neurodégénératives-UMR 5293, CNRS, CEA, University of Bordeaux, Bordeaux, France

6 Brain Connectivity and Behaviour Laboratory, Paris, France

Running Head: BRAIN ENERGY MANAGEMENT IN MITOCHONDRIAL DISEASE

* Correspondence to Tor Wager, Martin Picard and Ke Bo：Tor.D.Wager@dartmouth.edu, martin.picard@columbia.edu, Ke.Bo@dartmouth.edu

Abstract

Brain function relies on energy supplied by mitochondrial energy transformation, but how cellular energetics constrains neurological function and cognition remains poorly understood. Genetic defects in mitochondrial DNA cause rare mitochondrial diseases (MitoD) that offer a unique window to examine how mitochondria affects the brain and cognition, and the possibility to identify neural processes that are most energetically constrained. In this study, we assessed functional magnetic resonance imaging (fMRI) on 29 participants with MitoD and 62 matched controls during resting state and tasks probing cognitive (N-back task), affective (cold pain), and sensory (multisensory visual and auditory perception) functions. MitoD individuals exhibited significant cognitive deficits across a range of functions, including executive function and working memory, mental and physical fatigability, low exercise tolerance, and low mood. As expected, these deficits were accompanied by markedly elevated blood levels of metabolic stress markers, including GDF15 and FGF21. Surprisingly, overall BOLD fMRI activity and connectivity were largely intact across all tasks in MitoD individuals. However, those with more severe cognitive impairment and higher GDF15 levels showed reduced working memory-related BOLD activity, which in turn mediated poorer task performance. Conversely, individuals with relatively preserved cognitive function exhibited hyperactivation in working memory regions and working memory performance compared to controls, suggesting compensatory engagement of cortical systems in high-functioning MitoD individuals. These effects were weaker in the sensory domain and absent during affective (cold pain) processing. These data suggest that when mitochondrial energy transformation is limited, the brain operates an energy hierarchy that prioritizes essential functions such as affective responses while downregulating more energy-demanding, complex cognitive processes.

Introduction

The human brain accounts for 20-24% of the body's energy consumption while representing only about 2% of total body mass [1–3]. This large and constant energy requirement underpins critical neural processes such as synaptic transmission, plasticity, and large-scale network coordination, which together support brain functions ranging from basic sensory perception to complex cognitive and affective regulation [4]. While cellular and animal studies have long established the critical role of energy metabolism in neural function [5,6], recent human research increasingly highlights metabolic health as essential for human mental functioning [7–9]. Bioenergetic abnormalities are now recognized across diverse psychiatric and neurological disorders including major depressive disorder [10], psychotic disorders [11], autism spectrum disorders [12], bipolar disorder [13], as well as neurodegeneration diseases including Alzheimer disease [14] and Parkinson disease [15]. Despite this growing evidence and the urgent need to elucidate specific neural mechanisms linking metabolism and brain function [16], directly translating these insights into human neuroscience remains challenging due to the limited availability of non-invasive methodologies for assessing or manipulating brain bioenergetics in vivo.

Mitochondria are central to cellular energy metabolism–they transform oxygen and food substrates into usable energy, and also serve as intracellular processors through dozens of interrelated functions [17,18]. Mitochondria generate adenosine triphosphate (ATP) via oxidative phosphorylation, providing the energy required to sustain the high demands of neurons and glial cells, fueling intracellular processes such as ion transport, endocytosis, and neurotransmitter biosynthesis and reuptake, among others [19]. The human brain contains distinct populations of mitochondria subserving a spectrum of energy demands and bioenergetic requirements, including more mitochondria specialized for energy transformation in metabolically-demanding areas [20,21]. Impaired mitochondrial energy transformation can disrupt synaptic transmission and ultimately compromise neuronal survival [22], alter gene expression [23] and neurogenesis [24,25], and therefore compromise brain functions. In terms of behavior, in animal models mitochondrial biology regulates anxiety [26], memory [27], dominance and social behaviors [28,29]. Thus, mitochondrial perturbations provide a unique window into understanding how brain functions and associated behaviors are shaped by cellular energy metabolism.

Mitochondrial diseases (MitoD) represent extreme cases of mitochondrial defects caused by mutations or deletions in the mitochondrial DNA (mtDNA). Among the most common

mtDNA defects are the point mutation m.3243A>G in a transfer RNA gene, or single, large-scale deletions that commonly affect multiple mtDNA genes [30,31] (mutations in autosomal genes in the cell nucleus also cause MitoD [32]). mtDNA defects cause morphologic and functional abnormalities in mitochondria that decrease energy flux through the brain-mitochondria circuitry [33], impairing multiple mitochondrial functions. Consequently, patients exhibit a spectrum of neurological symptoms, including cognitive impairment, psychiatric disturbances, and sensory deficits [32,34–36]. Because mitochondrial defects directly compromise cellular energy metabolism, MitoD populations offer a natural opportunity to clarify the mind-mitochondria relationships, analogous to studies using focal brain lesions to clarify structure-function relationships [37,38,39]. By comparing MitoD and individuals with healthy mitochondria, we can get at metabolism-function relationships, with the caveat that deficits may drive chronic developmental or acute compensatory adaptations. Despite the immense research potential on this population, research on MitoD has predominantly focused on pathological, neurological, and other organ impacts on a clinical level [40–43]. Functional neuroimaging studies involving multiple brain functions together with deep multi-modal phenotyping in this rare population remain scarce. The Mitochondrial Stress, Brain Imaging, and Epigenetics (MiSBIE) study [101] addresses this gap.

One key concept examined in this paper is the notion of Energy Constraints (EC). This refers to the notion that energy depletion or diversion can prevent normal or optimal functions – even in the absence of structural or functional alterations – and that energy can be depleted by disease-related processes that over-consume energy [44]. This principle is based on fundamental bioenergetic constraints that operate across all levels of life [45]. If a biological unit — a brain region, an activated cell type, or an organ — costs more energy than it should under optimal health conditions, it becomes “hypermetabolic” and steals energy away from other functions, a process called energy trade-offs [46]. Consistent with this logic, mitochondrial defects like those causing MitoD produce cellular hypermetabolism in cells [47] and systemic hypermetabolism in affected patients [48]. We hypothesize that this results in energy trade-offs relevant to health and cognition, although this question has not been directly addressed.

The current study provides, to our knowledge, the first systematic functional MRI (fMRI) investigation examining the relationship between bioenergetic deficits and brain function across multiple cognitive and functional domains in the MitoD population. Our approach spans resting-state, sensory, affective, and cognitive domains using: (1) a multisensory checkerboard+tone task, (2) a cold pain task, and (3) a working memory (WM) task. We chose WM task because it is both highly ATP-demanding[49]—making it sensitive to mitochondrial constraints—and central

to executive control and fluid intelligence [50,51]. We build up multiple models to extract spontaneous and task-related brain network activation and compare them between control participants and those with MitoD. We hypothesize that mitochondrial defects may manifest in two potential ways. First, the MitoD-related deficits in ATP production could lead to impaired synaptic activity [52], which might cause global impairments in brain functions, including sensory, cognitive, and affective domains, and spontaneous resting-state activity. Alternatively, due to energy-based competition driving energy constraints, some fundamental brain functions for sustaining life-critical processes might be indispensable, such as maintaining spontaneous brain activity and affective processing. Thus, the brain may preferentially allocate its limited energy resources to the essential operations [53], leaving less energy available for functions that, while energy-intensive, are less fundamental, such as working memory. We tested these competing hypotheses by comparing resting-state and task-related fMRI activity and connectivity between MitoD patients and healthy controls.

Results

Multidimensional characterization of the mitochondrial disease phenome

To provide an initial characterization of the MitoD phenome and identify key deficits with large effect sizes, we compared 70 healthy controls with 40 MitoD patients (91 of the participants have available MRI data; see *Methods* for details) across assessments of cognitive function, psychosocial variables including personality, mental health, mental and physical fatigability, molecular biomarkers derived from blood, daily behavior, disease related symptom severity, and clinical measures of neurological, physical, and cognitive function [101]. As shown in Figure 1A, MitoD patients exhibited substantial deficits in a range of cognitive, functional, and physiological variables, with at least medium effect sizes in many cases (absolute Hedge's $g > 0.5$). In Figure 1A and below, we report the measurements that survived false discovery rate (FDR correction) ($q < 0.05$) for multiple comparisons (See Table S1 for detailed statistics. E.g. p value before and after FDR correction). Molecular signaling factors in blood included elevated Growth Differentiation Factor 15 (GDF15; Hedge's $g = 1.7$) and Fibroblast Growth Factor 21 (FGF21; $g = 1.34$) in MitoD compared to control, both critical biomarkers indicative of impaired cellular metabolism [54–56]. Additionally, MitoD patients showed elevated lactate ($g = 1.05$), glycosylated hemoglobin ($g = 0.84$), blood urea nitrogen (BUN, $g = 0.69$), elevated total lymphocyte count (g

= 0.51), and decreased chloride levels (g = 0.6), indicating compromised mitochondrial oxidative phosphorylation and a broader of physiological disturbances across metabolic, electrolyte, immune and acid-base balance typically seen in mitochondrial disorders [57].

Compared to controls, MitoD patients also demonstrated pronounced impairments in cognitive performance, physical activity, and fatigability. On neuropsychological tests, patients performed worse on numeric sequencing, letter sequencing (RBANS trail making subtest), word reading, and inhibition tasks (g = 0.64, 0.58, 0.52, and 0.48, respectively, D-KEFS Color-Word Interference subtest), and scored lower on openness in the personality test (g = 0.52, NEO Five-Factor Inventory). Patients further reported heightened physical (g = 1.23), cognitive (g = 1.00), and psychological fatigue (g = 0.99)assessed by the Pittsburgh Fatigability Scale—which quantifies fatigability in relation to a defined activity. Patients also reported pupillomotor symptoms (g = 1.30, COMPASS-31). Thus, consistent with the literature and with the presence of mitochondria in every tissue and organ of the body, MitoD patients typically show multi-system clinical deficits.

Moreover, MitoD patients exhibited substantial abnormalities across a comprehensive battery of clinical assessments evaluating disease symptoms and neurological health, including the Newcastle Mitochondrial Disease Adult Scale (NMDAS; g = 1.65; an index of adult mitochondrial disease–specific symptoms), the Columbia Neurological Score (CNS; g = 1.61; an index of neurological health across multiple domains), the Karnofsky Performance Scale (KPS; g = 1.83; an index of functional impairment), the Composite Autonomic Symptom Score (COMPASS; g = 1.01; an index of multi-system autonomic function), the sit–to–stand test (test of lower body power, balance, and endurance) (g = 0.70), and Forced Vital Capacity (FVC; g = 0.52; an index of lung function) (see *Methods* for detailed descriptions of these tests). Some of the largest single-item effects within these indices included impaired exercise tolerance (g = 1.07), ocular-function measures such as chronic progressive external ophthalmoplegia (g = 1.24) and ptosis (g = 1.22) from the NMDAS, and dysfunction in cranial nerves III, VI, and IV from the CNS (g = 1.51, 1.44, and 1.37, respectively), which regulate eye movement and pupil response, together indicating broad neurological involvement.

A summary of associations among these items across participants is shown in Figure 1B–C. To explore the functional grouping of these features, we first used a permutation test to determine the optimal number of clusters (Wager et al., 2008), which was three in the current dataset. We then applied hierarchical clustering analysis, which identified three distinct clusters (Figure 1B),

each assigned a different color; the correlation matrix was sorted accordingly (Figure 1C). The results revealed structured patterns of association among variables: Cluster 1 (Blue) primarily consisted of measures related to metabolic rate and lung function, as well as plasma and saliva cell-free DNA (both mitochondrial and nuclear, mtDNA ND1 and nDNA B2M genes, respectively) measured at multiple time points. Cluster 2 (Orange) included personality traits, cognitive performance and dysfunction tests, serum cell-free DNA levels, and metabolic indicators such as sodium, chloride, and creatinine. Cluster 3 (Green) included adversity exposure and negative affective symptoms (e.g., depression, anxiety, childhood trauma, burnout), fatigability scores, autonomic symptoms, and key cellular and molecular biomarkers including GDF15, FGF21, lactate, glucose, HbA1c, and insulin (with the first three measured at multiple time points). In general, items from Cluster 3—such as GDF15, lactate, negative psychosocial experience, and fatigability —were negatively correlated with items in Cluster 2, including social support, cognitive ability, and neurological and physical health (see Supplementary Table S1), reflecting an overall antagonistic relationship between physiological and psychological markers of metabolic deficits and resilience-promoting psychosocial and behavioral factors (Udeh-Momoh et al. 2025).

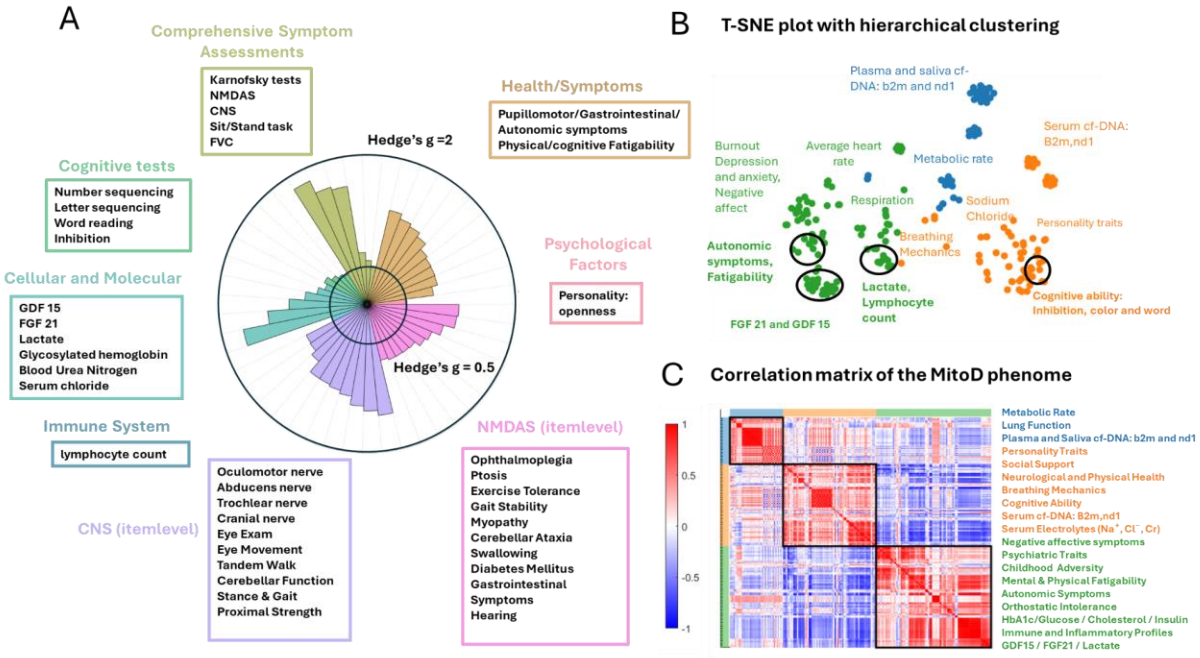

Figure 1. Overview of phenotypic domains and their interrelationships in the current study.

A) Effect sizes (Hedge's g) comparing mitochondrial disease (MitoD) patients to healthy controls across five key domains: cognitive tests, physical activity, autonomic symptoms, composite symptom assessments, and cellular/molecular markers. The tested variables with FDR $q < 0.05$ are shown in the wedge plot. The wedge plot displays the measurements that show significant differences between the MitoD and control groups and survive FDR correction at $q < 0.05$. Notably, two of the most representative comprehensive symptom assessments—the Newcastle Mitochondrial Disease Adult Scale (NMDAS), which evaluates mitochondrial disease–specific symptoms, and the Columbia Neurological Score (CNS), which evaluates general neurological health—are decomposed into single-item levels and displayed individually. The top ten individual items from each of these scales that surpass FDR correction at $q < 0.05$ are also presented. **B)** t-SNE visualization of all measurements, with clusters defined by hierarchical clustering and color-coded accordingly. These clusters reflect coherent domains such as metabolism, psychosocial experience, cognitive function, and molecular markers. Measurements that remain significant after FDR correction ($q < 0.05$) are circled and bolded. **C)** Correlation matrix of all measurements using Spearman correlation, with hierarchical clustering used to sort the variables. Red and blue indicate positive and negative correlations, respectively, highlighting distinct phenotypic clusters and cross-domain associations. Note: the corresponding correlation and clustering analyses are performed on the whole dataset, including both MitoD and control populations. For MitoD-specific correlation analysis, see Supplementary Figure S1.

Task-evoked brain activity

MitoD vs Control group comparison

To probe common brain functions across sensory, affective, and cognitive domains, we modeled task-evoked hemodynamic responses relative to rest. As shown in Figure 2, each task induced robust, expected patterns of significant brain activation collapsing across MitoD and Control groups (FDR $q < 0.05$, cluster size >=10 voxels). The N-back working memory task elicited activation in frontal-parietal regions, striatum, cerebellum, midbrain, and visual cortices, with spatial correlations aligning closely with established working memory patterns (via Neurosynth topic maps), as shown in Fig. 2A. The cold pain task activated the posterior and anterior insula and overlying operculum, anterior mid-cingulate, striatum, superior cerebellum, and thalamus (Fig. 2B). Finally, the multisensory task elicited strong responses in early visual and auditory cortices and lateral prefrontal regions (Fig. 2C).

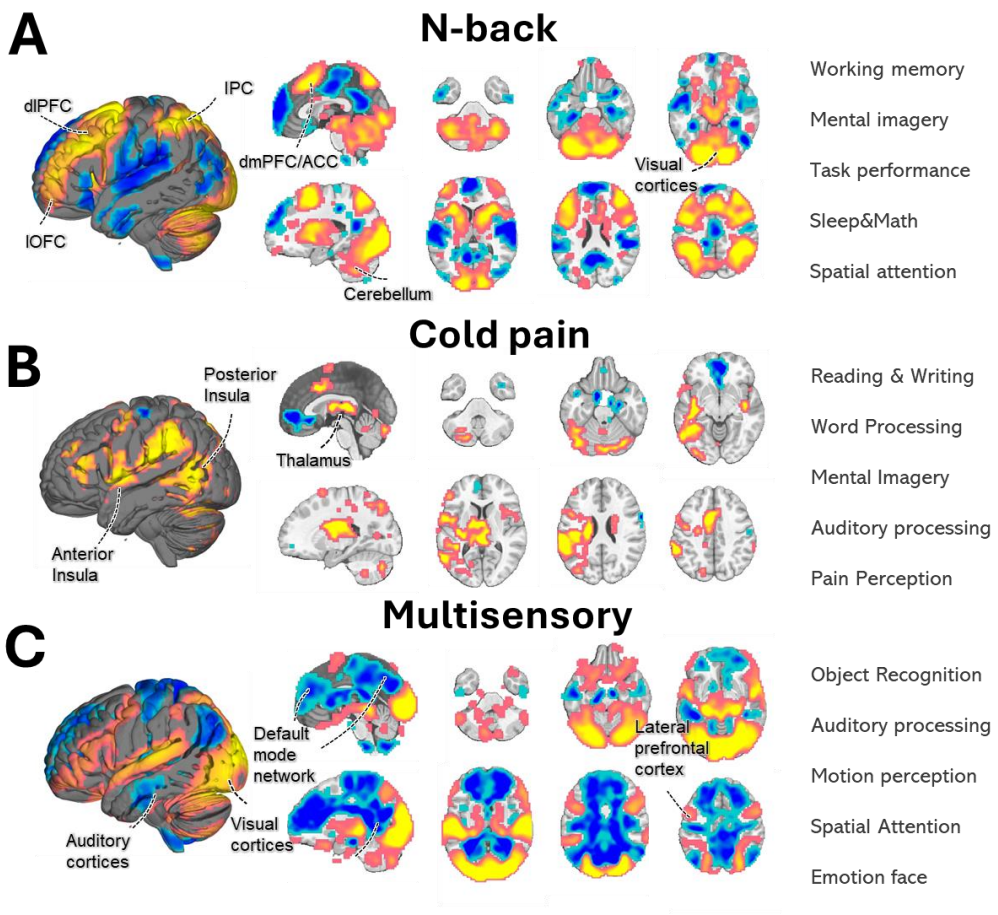

Figure 2. Whole-brain activation for the three tasks. The left panel shows task-related activation after controlling for multiple comparisons (FDR-corrected, $q < 0.05$, cluster size > 10). The right panel displays the five most correlated Neurosynth forward inference topic maps from a set of 54 Psychological topics [58,59]. **A)** N-back task activation: 2-back vs. 0-back. **B)** Cold pain task activation: Cold wrapper on right forearm vs. room temperature wrapper on right forearm. **C)** Multisensory task activation: Visual checkerboard and audio task vs. rest.

To construct single measures that maximally capture task-related activity for each task, we trained paired support vector machine (SVM) classifiers using leave-whole-participant-out cross-validation to distinguish task vs. rest blocks within each task. Classification accuracies were high for the multisensory (98.24%, d = 2.18), cold pain (87.12%, d = 0.92), and N-back (97.0%, d = 1.67) tasks, indicating the reliable detection of task-induced activations across participants. Figure 3B shows voxels with significant, reliable weights across 5000 bootstrap samples (See

Figure S2 for $p < 0.05$ uncorrected weight maps). These task-related neuromarkers allowed us to calculate individual-level brain pattern expression scores and conduct a test for MitoD vs. Control differences in task-related activity with >80% accuracy for each task (see Methods and Figure 3A). Compared to univariate analyses, these multivariate neural signatures are less susceptible to noise and provide richer, population-level information, thereby yielding more robust estimates of individual differences in task-evoked brain responses. [60–62].

As shown in Figure 3C, two-sample t-tests revealed no significant group differences between MitoD and Control for any task: multisensory ($t = 0.54$, $p = 0.59$, df= 88, $BF_{01} = 0.26$), cold pain ($t = –0.11$, $p = 0.59$, $n = 89$, $BF_{01} = 0.23$), and N-back ($t = 0.33$, $p = 0.74$, df = 72, $BF_{01} = 0.26$). Note that in the current and subsequent analyses of working-memory brain representations, we excluded 14 participants with task accuracy below 40% (chance = 50%) or missing task responses, yielding a final total sample of n = 74 and MitoD sample of n = 25 (See methods for more details). Equivalent analysis without these exclusions are reported in Supplementary Figure S3 and produces the consistent conclusions with original analysis. The Bayes factor (BF_{01}) quantifies the relative evidence for the null hypothesis versus the alternative by comparing their marginal likelihoods [63]; values below 1 indicate stronger support for the null. In our analyses, $BF_{01} = 0.26$, 0.23, and 0.54 for the multisensory, cold pain, and N-back tasks, respectively, further supporting the absence of any group differences.The lack of group differences was paralleled by null effects in behavioral performance (in N-back task accuracy) between MitoD patients and controls ($T = -1.55$, $p = 0.13$, $BF_{01} = 0.67$, as shown in figure 4A). These findings indicate that overall task-related brain responses are not significantly different in MitoD relative to controls.

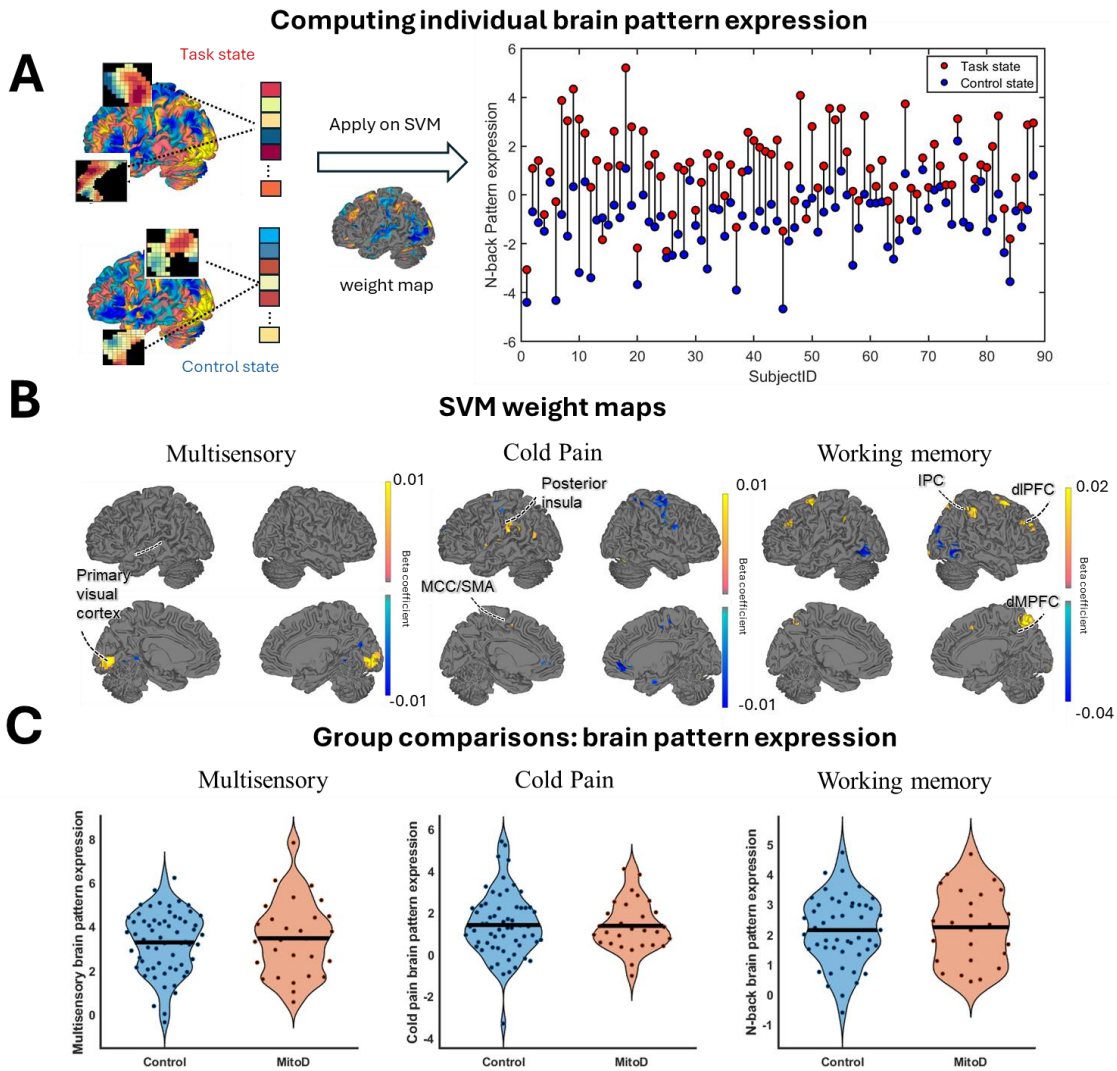

Figure 3. Using a support vector machine (SVM) to extract task-related brain pattern expression at the individual level. **A)** Example procedure using the N-back task to compute brain pattern expression at the individual level. Specifically, whole-brain maps of two contrast conditions were extracted from each participant as feature vectors. These vectors were then applied to the SVM weight map using a dot product. As a result, each participant received two brain pattern expression scores, one for each condition. The difference in pattern expression between task and control was used to quantify task-related brain activation at the individual level. Nearly all participants exhibited higher pattern expression in the N-back vs. control condition, corresponding to 98% classification accuracy in a forced-choice test. **B)** SVM weight maps for each task, bootstrapped 5,000 times to highlight significant weights. Weight values from whole-brain voxels were used to compute brain-pattern expression. For display purposes, we show FDR-corrected ($q < 0.05$) maps for the multisensory and N-back tasks, and an uncorrected ($p < 0.001$) map for the cold pain task. **C)** Violin plots comparing brain task expression between MitoD and control

groups. Dots represent participants, and values above zero indicate positive brain representation for the task vs rest contrast, which refers to a correct classification.

Disease Severity Predicts Brain and Behavioral Variability in MitoD

Though the groups showed similar levels of brain activity and performance overall, MitoD patients vary substantially in disease severity. Therefore, we assessed whether individual differences in physical functional impairments indexed by the global disease severity NMDAS scores were related to individual differences in N-back performance and brain responses. For any correlation analysis involving NMDAS scores, we used Spearman's rank correlation due to the non-normal distribution of those scores. As shown in Figure 4B, MitoD patients with higher disease severity showed lower N-back fMRI pattern expression ($r = –0.68$, $p < 0.001$) and lower behavioral performance ($r = –0.49$, $p = 0.01$). These relationships remained significant after controlling for age (brain: $r = –0.67$, $p < 0.001$; behavior: $r = -0.46$, $p = 0.024$). Together, these findings indicate that greater disease severity is associated with reduced working-memory network activation and poorer task performance.

Mediation analyses indicated that disease severity mediated the relationship between mitochondrial genotype (Control vs. MitoD) and each of task-related brain activation and behavioral performance (Figure 4C). As shown in Figure 6C, NMDAS scores partially mediated the effect of genotype on N-back fMRI pattern expression with a significant indirect effect ($ab = 0.58$, $SE = 0.22$, $p < 0.001$) and a significant direct effect ($c' = –0.69$, $SE = 0.29$, $p = 0.03$), and fully mediated the effect of genotype on N-back behavioral performance with significant indirect ($ab = 0.053$, $SE = 0.023$, $p = 0.007$) and non-significant direct effect ($c' = –0.0077$, $SE = 0.034$, $p = 0.78$). Thus, disease severity fully accounts for the genotype-related deficits in working-memory performance and substantially mediates, but does not entirely explain, the genotype-related reductions in N-back brain activation, revealing both pathological and compensatory mechanisms in MitoD.

This pattern of findings suggests the presence of a subgroup of resilient MitoD patients who, in spite of having genetic mitochondrial defects, show intact or even enhanced working memory-related brain activity relative to controls. The presence of subgroups was also indicated by examination of the distribution of NMDAS scores, which appeared to be bimodal, with one group scoring between 0-15, in the range of controls, and the other scoring between 22-40, clearly more impaired. We applied a data-driven K-means clustering approach to objectively subdivide the MitoD group into mild (resilient) and severe (susceptible) categories, allowing the algorithm

to determine the boundary. As shown in Figure 4D, the resilient (mild-disease) subgroup showed comparable behavioral performance to healthy controls (t = 0.23, p = 0.82, df = 64) but significantly higher working memory-related brain activation than controls (t = 1.97, p = 0.05, df = 64). In contrast, patients with severe disease exhibited significantly reduced brain activation (t = -2.47, p = 0.02, df = 55) and impaired behavioral performance (t = -3.7, p < 0.001, df = 55) compared with controls. We interpret these findings as a potential compensatory mechanism whereby resilient MitoD patients exhibit greater neural engagement to maintain behavioral performance comparable to controls, while severely affected patients are unable to compensate and thus exhibit reduced brain activation and impaired task performance.

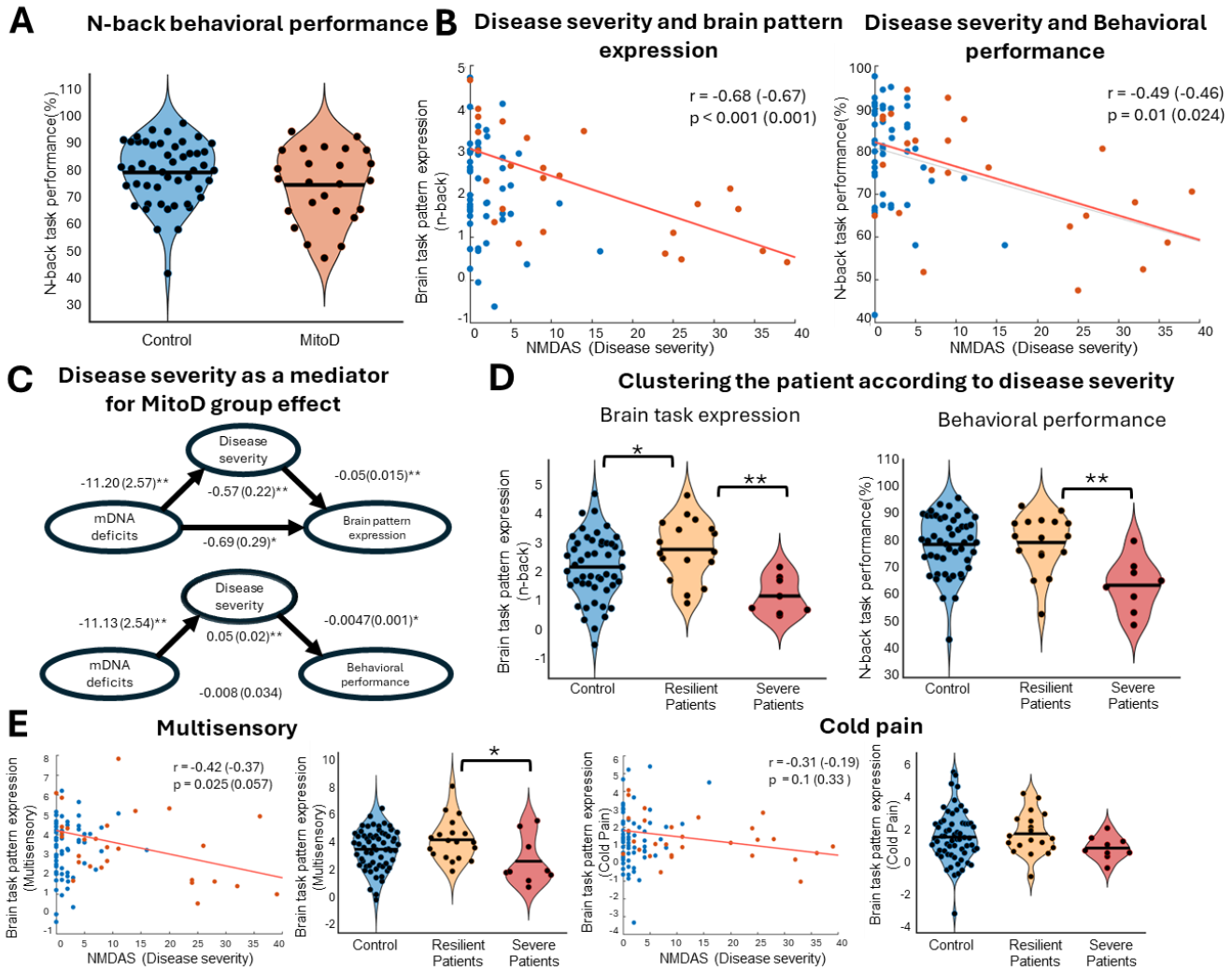

Figure 4. The influence of mitochondrial disease severity on brain activation and behavioral performance (N-back task only). **A)** Comparison of N-back task performance between MitoD and control groups. **B)** Correlations between disease severity and brain pattern expression (left), and between disease severity

and task performance (right) within the patient group (orange). Results controlling for age are reported in parentheses. **C)** Mediation analysis testing whether disease severity mediates the relationship between mitochondrial DNA (mtDNA) deficits (MitoD vs. control) and brain pattern expression (top) or behavioral performance (bottom). Disease severity significantly mediated both relationships, partially for brain expression and fully for behavioral performance. **D)** The MitoD group was divided into two subgroups based on disease severity using K-means clustering. Average brain pattern expression (left) and behavioral performance (right) were compared within subgroups and with control groups. **E)** Parallel analyses from panels B and D were conducted for brain pattern expression in the cold pain and multisensory tasks.

Task-Specific Effects of Disease Severity

To compare the relationship between mitochondrial genotype, brain activity, and disease severity across tasks, we performed correlation and mediation analyses on task-related fMRI pattern expression scores for the multisensory and cold pain tasks. Performance data were not collected for these tasks, precluding behavioral analyses. In the multisensory task, a similar but weaker compensatory trend was observed in brain scores. Disease severity predicted lower brain pattern expression ($r = -0.42$, $p = 0.025$), though this relationship became marginal after correcting for age ($r = -0.37$, $p = 0.057$). Disease severity did not mediate the relationship between mitochondrial genotype and brain activity scores. In the subgroup analysis of brain pattern expression, significant difference is only found between resilient vs severe patient ($t = 2.4$, $p = 0.023$, $df = 26$), while resilient MitoD patients only showed marginally higher brain pattern expression compared to controls ($t = 1.82$, $p = 0.07$, $df = 79$), and severe patients did not show significantly lower scores compared to control ($t = -1.67$, $p = 0.10$, $df = 69$) (Figure 4E left). In contrast, the affective (cold pain) task did not reveal any significant associations with disease severity (Figure 4E right).

Finally, a Bayes factor analysis comparing evidence for a non-zero versus null severity–brain correlation yielded $BF_{10} = 117$ for working memory (strong evidence), $BF_{10} = 0.94$ for multisensory (weak evidence), and $BF_{10} = 0.23$ for cold pain (evidence favoring the null). These findings point to selective effects of disease severity on working memory, and are consistent with the notion of a hierarchical prioritization of function under energetic constraints [44–46]: critical functions such as affective processing (cold pain) may be preserved under energy constraints, while high-energy-demand but less survival-critical functions like working memory are more vulnerable to impairment.

Resting state brain activity

Beyond task-related activity, spontaneous brain activity, including within large-scale resting-state networks like the default mode network and the frontoparietal network, accounts for a substantial portion of the brain's energy consumption [2,64,65]. To assess how mitochondrial MitoD-related energy transformation defects influence this activity, we examined spontaneous neural fluctuations using Amplitude of Low Frequency Fluctuation (ALFF) and Regional Homogeneity (ReHo) [66,67].

No significant group differences were observed between MitoD patients and healthy controls at FDR-corrected $q < 0.05$. However, at a more liberal threshold ($p < 0.001$ uncorrected, cluster size > 20 voxels), the MitoD group showed lower ALFF in the cerebellum and higher ReHo in the dorsomedial and ventromedial prefrontal cortices (dmPFC and vmPFC) (Figure 5A). We further tested whether disease severity, measured by the Newcastle Mitochondrial Disease Adult Scale (NMDAS), correlated with ALFF or ReHo within the MitoD group. No associations were significant at $p < 0.001$ level. Similarly, when we compared average ALFF and ReHo across seven canonical resting-state networks (Yeo et al., 2011), we found no significant differences between MitoD and Controls or correlations with NMDAS, thus ruling out an overall spontaneous activity abnormality caused by MitoD.

Next, we compared resting-state functional connectivity differences between MitoD patients and controls among the same seven networks (Figure 5B), controlling for participant-wise head motion (average framewise displacement). Robust regression revealed selective increases in connectivity in the MitoD group at uncorrected thresholds ($p < 0.05$) for connections between (a) frontoparietal and somatosensory networks, and (b) frontoparietal and ventral attention networks. However, these results did not survive correction for multiple comparisons at FDR $q<0.05$. We also computed connectivity across 518 gray-matter parcels defined based on widely used atlases of the cortex, basal ganglia, thalamus, and brainstem (Supplementary Figure S4), but again found no FDR-corrected differences; qualitatively, there was a trend toward increased cortical-to-cortical connectivity in MitoD patients, which decreased further with greater disease severity.

In summary, these results from rare individuals with genetic mitochondrial defects do not appear to cause strong or widespread alterations in spontaneous brain activity or network-level connectivity at rest. These measures also did not correlate with disease severity, indicating intact hemodynamic responses and connectivity overall.

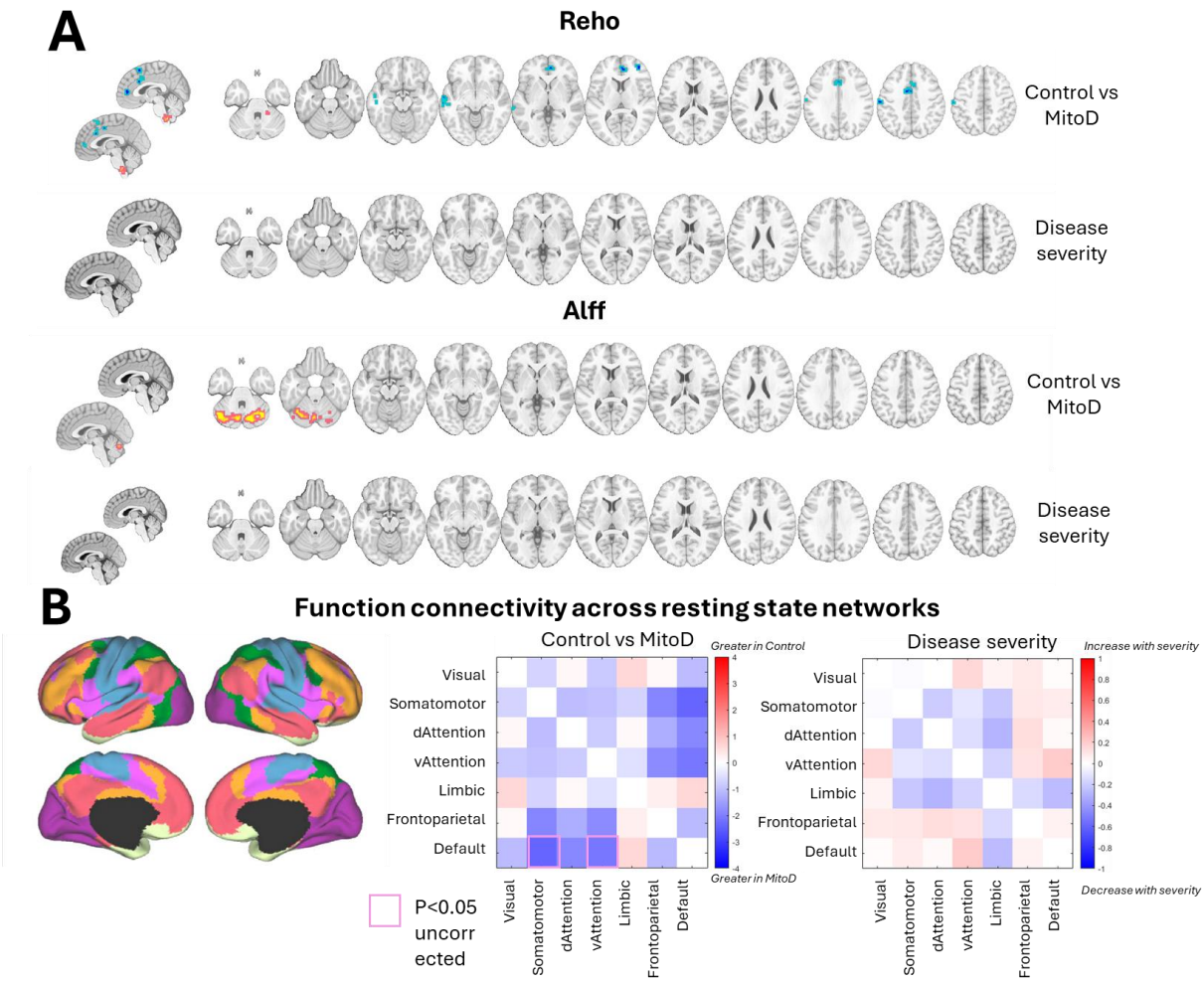

Figure 5. Resting-state fMRI analyses reveal limited group-level effects. **A)** Group comparison maps for Regional Homogeneity (ReHo) and Amplitude of Low Frequency Fluctuations (ALFF) between mitochondrial disease (MitoD) patients and healthy controls (top row), as well as correlations with disease severity within the MitoD group (bottom row). Voxel-wise threshold set at uncorrected $p < 0.001$ with cluster size > 20. No clusters survived FDR correction. **B)** Functional connectivity analysis across seven canonical resting-state networks defined by the Yeo et al. (2011) atlas (left). Group-level connectivity

matrices (right) show between-network connectivity for controls vs MitoD (middle) and associations with disease severity (right). Most effects did not reach statistical significance, indicating minimal alterations in resting-state connectivity in MitoD.

The energetic stress marker GDF15 and brain function

Functional measures of MitoD disease severity may be paralleled by systemic processes related to mitochondrial function and cellular metabolism detectable in blood and other tissues. If so, blood or salivary biomarkers related to these processes could provide indices of systemic mitochondrial health in MitoD and even beyond, as well as targets for prevention and treatment efforts. Among potential circulating biomarkers, GDF15 is the most robust marker of MitoD [57,68]. GDF15 also is a stress-responsive cytokine increasingly recognized as a marker of cellular and mitochondrial energetic stress [69]. Blood GDF15 meets several key criteria for a marker of systemic energetic stress: (1) it is the most dramatically elevated circulating protein with aging; (2) it is induced by mitochondrial-targeting drugs including metformin; and (3) its levels increase in many chronic conditions—including cardiovascular disease, cancer, mood disorders, Alzheimer's disease, and autoimmune disorders [69,70].

In the current study, plasma GDF15 was substantially higher in MitoD patients than controls ($t = 6.1$, $p < 0.001$; see Figure 6A) and strongly correlated with NMDAS disease severity in MitoD ($r = 0.75$, $p < 0.001$), replicating previous findings using the same dataset[71] (reproduced analysis). The effect sizes were comparable to those of composite clinical batteries like the NMDAS and CNS and large enough to separate patients from controls, achieving an area under the ROC curve of >0.85 [71]. These evidence and others reviewed elsewhere (Picard and Murugan 2025) suggest GDF15 has the potential to serve as a broader index of mitochondrial energetic stress that can be applied in both control and MitoD populations.

Unlike disease severity—which is only relevant to MitoD patients—GDF15 is non-zero in controls and reflects their relative mitochondrial energetic stress level. Therefore, we tested whether GDF15 levels were associated with working memory–related brain activity and task performance across the entire sample. As shown in Figure 6B, higher GDF15 levels predicted reduced N-back brain pattern expression across the entire sample ($r = –0.48$, $p < 0.001$), controlling for Group (MitoD vs. control). Within each group, this relationship remained significant (patients: $r = –0.64$, $p = 0.003$; controls: $r = –0.41$, $p = 0.004$). Similarly, higher

GDF15 levels predicted poorer behavioral performance on the N-back task across the whole cohort (r = –0.33, p = 0.007), controlling for Group. Because GDF15 is produced by non-brain tissues and signals, possibly exclusively on the brainstem to alter behavior ((Lockhart et al. 2020; Engström Ruud et al. 2024)) consistent with the notion that peripheral signals of energetic stress are expected to suppress energetically-expensive brain functions [72]. The effect sizes were comparable in controls (r = –0.33, p = 0.02) and in MitoD patients (r = –0.36, p = 0.12), although the latter did not reach significance, likely due to its smaller sample size. Together, these results highlight GDF15's potential as an effective biomarker of metabolic health relevant for tracking brain activity and cognitive performance under energy demanding task.

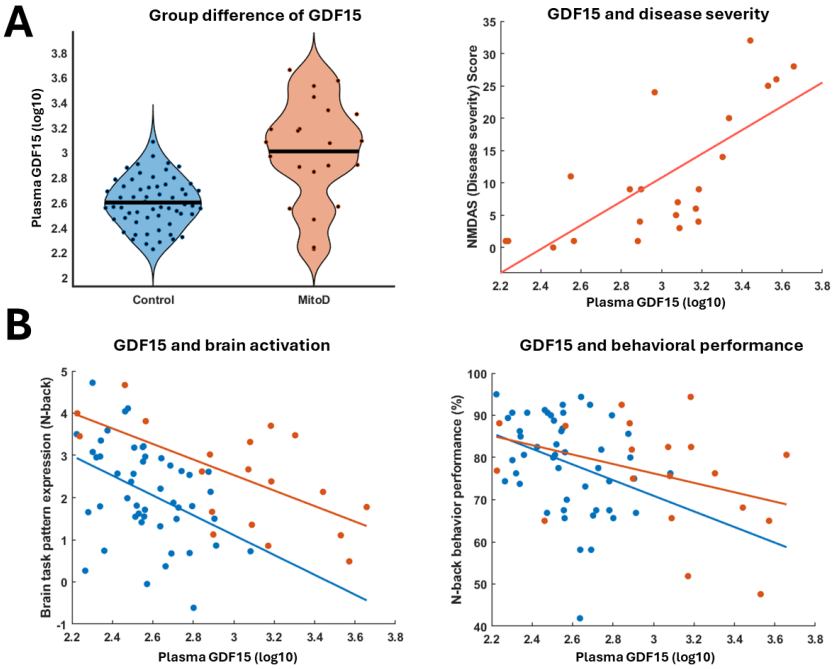

Figure 6. GDF15 as a potential biomarker linking mitochondrial bioenergetic dysfunction to cognitive deficits tested by brain and behavioral measurements. **A)** Validation and reproduced analyses demonstrate that plasma GDF15 (log-transformed) robustly differentiates the MitoD population from normal controls and is significantly associated with NMDAS disease severity within the MitoD group, replicating findings published in a previous study using the same dataset[71] **B)** Relationships between plasma GDF15 and working-memory outcomes are shown in two panels. Left panel: Correlation (Pearson) with brain-pattern expression during the N-back task—whole group: r = 0.48, p < 0.001; MitoD: r = 0.64, p = 0.003; Control: r = 0.41, p = 0.004. Right panel: Correlation with behavioral performance—whole group: r = 0.33, p = 0.007; MitoD: r = 0.36, p = 0.12; Control: r = 0.33, p = 0.02. Data points are colored blue for controls and orange for MitoD patients.

GDF15 is highly related to age in humans where it increases exponentially with advancing age [73–75]. In the current data, Age was not correlated with Group ($r = -0.016$, $p = 0.89$), but was correlated with higher GDF15 ($r = 0.38$, $p = 0.001$). Therefore, we further tested whether the GDF15 is able to predict working memory brain/behavior performance independently from the age effect. We tested two multiple regression models. Model 1 considered the main effects of Group (Control = 1, MitoD = -1), GDF15 (Log 10), and Age, and Model 2 tested a full model with their interactions.

In models predicting working memory–related brain activation, we found significant main effects of GDF15, age, and group in Model 1 ($t = –2.82$, $p = 0.007$; $t = –2.75$, $p = 0.007$; $t = –2.95$, $p = 0.004$, respectively; $df = 63$). No interaction effects in Model 2 reached significance. No interaction effects in Model 2 reached significance. These results indicate that, while aging is associated with reduced brain activation, higher levels of GDF15 account for additional variance in working memory–related activity, independent of age. Thus, metabolic health, as indexed by GDF15, may influence brain function independently from chronological aging.

In models predicting working memory–related behavioral performance, we found that only Age showed a significant main effect in Model 1 ($t = – 3.22$, $p = 0.002$, $df = 63$). In Model 2, two interaction terms were significant: Age × Group ($t = – 3.00$, $p = 0.004$, $df = 63$) and GDF15 × Group ($t = 2.02$, $p = 0.05$, $df = 63$). These results suggest two key points: 1) GDF15 does not predict behavioral performance independently of age across the full sample. 2) Both GDF15 and Age showed negative associations with behavioral performance overall, but their effects differ by group. The significant interactions indicate that in MitoD patients, compared to controls, GDF15 is stronger in predicting performance, whereas age is less influential. This suggests that factors beyond age, such as genetic influences, may play an additional role in shaping metabolic health and cognitive behavior in the patient group.

In sum, GDF15 emerges as a robust marker of systemic energetic stress that predicts brain activation and behavior during cognitively demanding tasks across the whole sample. Its association with brain activation appears only partly driven by age-related metabolic decline, while its relationship with behavioral performance is more strongly influenced by the aging process.

Discussion

Cellular energy transformation is critical to survival but also can become rate-limiting, meaning that insufficient energy flow relative to demands can impair function across all bodily systems, including the brain [44–46]. Rare human genetic mitochondrial defects provide a unique testbed to understand the influence of mitochondrial biology on human brain function and cognition. In the current study, we define the MitoD 'phenome' across clinical and psychosocial assessments and biomarkers in peripheral blood, and relate key clinical (NMDAS) and blood (GDF15) biomarkers to brain function at rest and across multiple tasks (working memory, multisensory, and cold pain). Overall, our findings show that despite widespread clinical deficits, brain function is remarkably preserved in MitoD patients, with intact BOLD activity and connectivity during tasks and rest. Impairments in brain activation and performance were selective to working memory and exhibited by a subgroup of patients with particularly strong clinical impairments and high levels of GDF15. Higher-performing MitoD patients were resilient to their genetic abnormalities, exhibiting a pattern of hyper-activation of relevant brain systems during working memory performance. These findings call attention to brain energetics as a potential driver of functional deficits and symptoms in mitochondrial diseases.

Mitochondrial disease phenome

By testing the MitoD population across blood biomarkers as well as clinical assessments, we found that patients exhibited marked cellular energy deficits, including elevated metabolic biomarkers (GDF15 and FGF21), disrupted oxidative phosphorylation indicated by elevated lactate, and systemic metabolic imbalances. These cellular disturbances were part of a broad cluster (Cluster 3) of correlated symptoms that included metabolic markers such as those mentioned above; psychosocial measures, including fatigability, depression, and anxiety; and physiological measures, including autonomic reactivity. The metabolic indicators in Cluster 3 were also negatively correlated with measures of social support, cognitive ability, and neurological/physical health (particularly executive function) in Cluster 2.

This pattern illustrates the broad, pervasive effects of mitochondrial disease, spanning molecular to cognitive levels. Beyond the marked elevations in metabolic biomarkers, increased HbA_1c and lactate suggest impaired mitochondrial oxidative phosphorylation, a compensatory shift to anaerobic glycolysis [76], and paralleled dysregulated glucose control [77]. These changes are also associated with reduced cognitive function in the elderly and schizophrenia populations [78,79]. Notably, similar bioenergetic shifts have been observed in healthy aging [80–82]—implying

shared mechanisms of metabolic decline in MitoD and normal senescence, which we will explore further alongside our GDF15 findings below.

Another key finding from our phenome analysis is that not all mental functions were equally impacted. MitoD patients showed no significant differences in overall personality traits—aside from reduced Openness—or in measures of negative affect symptoms. Within cognition, five tests yielded small effect sizes ($|g| < 0.2$), indicating little impairment. These included full-scale IQ (WASI), verbal learning and fluency without attention switching, semantic categorization fluency, and immediate story recall. These tasks are generally among those that, while placing demands on memory storage and recall, do not load highly on working memory (concurrent storage and processing) or executive function. In general, complex cognitive tasks (e.g., working memory or executive control) are more energetically costly than simpler tasks (e.g., sensory or motor processing), as they require widespread, recurrent network activation, multimodal integration, and greater neuromodulatory signaling. [49,83–85]. This selective profile contradicts the notion of a uniform cognitive downturn under energy deficit and echoes [36] findings that adult MitoD is characterized by focal deficits, particularly in visuospatial memory, attention, and executive functions, rather than global impairment [36]. This pattern is consistent with the idea that executive cognitive abilities are particularly energetically resource-limited.

Selective impairments in brain functions

Our neuroimaging findings are also consistent with a pattern of limited, focal deficits primarily in executive cognitive functions, and of brain metabolism as prioritized under energetic constraints. Patients with MitoD showed no overall reductions in BOLD responses during performance of multisensory, cold pain, or working memory tasks, and no differences in several resting-state brain functional connectivity measures after correcting for multiple comparisons. This lack of BOLD differences between MitoD patients and controls aligns with the efficiency-tradeoff hypothesis [86]: stimulus-evoked BOLD is powered primarily by aerobic glycolysis, which sacrifices ATP yield per glucose for rapid, information-rich signaling—so mild-to-moderate OxPhos impairments in MitoD leave these lower-cost circuits intact. Interestingly, we also did not observe connectivity differences selectively in cortical networks with high tonic metabolic demand, such as the fronto-parietal network and default mode network[64].

However, we observed a bimodal distribution of broad-based clinical impairment in MitoD, as defined by the composite NMDAS measure of disease severity. Patients with severe

mitochondrial bioenergetic dysfunction showed reduced engagement of the working-memory system, which overlaps substantially with the fronto-parietal network, and poorer working memory performance, along with higher GDF15. A resilient subgroup of MitoD participants exhibited supranormal, likely compensatory increases in activation, preserved performance, and lower GDF15. These effects were minimal in basic sensory processing and absent in affective pain processing, suggesting that under metabolic constraints, the brain prioritizes lower-cost functions, leading to selective impairment of more energy-demanding processes.

The finding of selective impairment is also in line with prior neuroimaging studies of MitoD, using structural MRI, DWI, and MRS [41,42]. These studies have demonstrated that, despite a global metabolic insult, brain pathology often manifests selectively, targeting specific regions or networks rather than causing diffuse structural alterations. Such selective impairment suggests two plausible, non-mutually exclusive mechanisms. First, intrinsic, spontaneous activity consumes the majority of the brain's energy budget (~60–80%) [87], while task engagement typically requires only a modest "top-up" of oxidative metabolism on the order of ~5% above resting levels [88]. In a healthy brain, this modest extra cost is readily covered by the available reserve, but in mitochondrial bioenergetic dysfunction—where ATP production for normal brain functions is drained from 'hypermetabolism' in maladaptive stress responses[46,47,48]—even a small incremental demand can exhaust that reserve, which potentially leads to abnormal brain activity during functional tasks. High energy-demand processes like working memory [49,83,84] therefore, selectively falter. Secondly, long-term mitochondrial bioenergetic dysfunction may stimulate adaptive neural plasticity, reallocating limited metabolic resources towards essential, survival-critical functions such as the construction of affective feelings and subjective value. Recent evidence supports the general principle that the brain can dynamically reallocate energy to meet pressing demands: for example, previous work[53] demonstrated an "attentional compensation" mechanism in healthy individuals whereby metabolic resources in the visual cortex were upregulated for attended stimuli and simultaneously downregulated for unattended information when task difficulty increased. By extension, in a chronic condition like MitoD, the brain may prioritize essential processes such as pain, basic sensorimotor function, and maintenance patterns of metabolism that underlie fluctuations in spontaneous activity, reducing the resources available for complex cognitive tasks.

Despite these results, it is important to note that the affective processing examined in our study reflects evoked responses to stimuli (e.g., cold applied to the arm) and does not imply that individuals with mitochondrial disease are immune to affective disorders. In fact, our phenome survey reports moderate or large effects on mood and affect, including fatigability, burnout, and depression (Supplementary Table S1), in the MitoD population. Previous studies have also reported a high prevalence of chronic pain and mood disorders in this population [89,90]. These longer-term affective disturbances may arise, at least in part, from deficits in the cognitive regulation of emotional responses—a process heavily dependent on fronto-parietal regions that overlap with those involved in working memory [59,91,92].

Potential biomarkers for studying Mitochondrial disease and brain activation

Among metabolic indicators, GDF15 emerged as a particularly important biomarker of metabolic health, with relevance beyond the patient population to healthy individuals. As in prior work (Huang et al., 2024a,b), we found GDF15 to be a highly sensitive indicator of mitochondrial energetic stress. Additionally, high GDF15 was associated with reduced working memory-related brain activation and behavioral performance in both MitoD patients and controls.
We also found a relationship between GDF15 and age, a key determinant of cognitive performance in healthy populations. We found that GDF15 increases with age, as in prior studies [75], and the relationship between GDF15 and both working memory-related brain activity and performance was reduced when controlling for age in healthy controls, implying that age and GDF15 effects on brain covary. This suggests that in the healthy population, aging is a primary source of increased energetic stress. Aging is associated with a progressive decline in cerebral energy metabolism, with neurons exhibiting high energy demands—such as those with extensive synaptic arborization—being particularly vulnerable [82], e.g., memory- and attention-related processes [82,93]. Notably, GDF15 explains additional variance in working-memory brain activity beyond chronological age, likely reflecting modifiable influences on metabolic and cognitive health, e.g., habitual physical activity [94] , educational Attainment [95] and diet [96].
In the MitoD population, age was no longer the primary factor influencing the relationship between GDF15 and working-memory–related brain activity, suggesting that age-independent factors may play a role. One key candidate is genetic factors—such as nuclear background interacting with mtDNA heteroplasmy—which strongly predetermine clinical trajectories, as demonstrated by monozygotic twin studies ([97]; reviewed in [98]). Environmental and lifestyle factors—diet, exercise, and hypoxic exposure—have also been shown in animal models to alter the course of mitochondrial disease [99]. Preliminary human data further suggest that

psychobiological factors, such as daily mood fluctuations, may influence symptom severity, and thus influence GDF15 and brain activation during complex tasks [100].
Looking ahead, studies employing GDF15 as a biomarker of metabolic burden should first establish whether its associations with brain function and clinical outcomes are age-related or age-independent, and then formulate research questions to examine additional genetic, environmental, and lifestyle factors that potentially influence metabolic and brain health.

Limitations

Despite the strengths of our multimodal approach, several limitations should be acknowledged. Although small for an fMRI study, our sample of 29 MitoD patients is among the largest functional neuroimaging cohorts in this rare-disease population, and effect sizes are large with many clinical and brain variables, conferring sufficient power for these very large effects. However, statistical power remains modest in detecting and characterizing associations with many variables with moderate or smaller effect sizes. Larger datasets are needed to more definitively rule out mitochondrial function-related changes in brain activity and connectivity.

Second, while we probed cognitive, sensory, and affective domains, our task battery does not encompass the full spectrum of energetically demanding brain functions, such as sustained attention, language processing, or explicit emotion-regulation paradigms. Future studies should include a wider array of tasks to determine whether the energy-hierarchy framework holds across additional neural systems.

Finally, although we statistically controlled for age, the strong correlation between GDF15 levels and age in healthy controls underscores the challenge of disentangling aging effects from mitochondrial health when interpreting metabolic biomarkers. Longitudinal designs and complementary measures of mitochondrial biology will be needed to clarify the independent contributions of chronological aging and energetic deficits.

Conclusions

In summary, genetic mitochondrial disease is characterized by elevated blood levels of the stress marker GDF15, along with other blood-based metabolic markers—which, in turn, are associated with multifaceted cognitive deficits, particularly impairments in sequencing and inhibition, as well as increased autonomic symptoms and fatigue. Though multifaceted, these deficits are focal rather than resulting from global cognitive dysregulation. In line with this pattern, overall brain BOLD activity and connectivity were largely intact across multiple tasks and connectivity metrics, but individuals with greater cognitive impairment and higher GDF15 levels exhibited reduced working memory-related BOLD activity, which in turn led to poorer task performance. Conversely, high-functioning MitoD individuals showed compensatory hyperactivation in working memory regions that supported relatively intact performance, characterizing a resilient phenotype that could be further studied to identify resilience-related factors. We found effects selectively in working memory and other tasks requiring executive function, but not in multisensory or cold pain processing, pointing to a potential energy hierarchy in the brain that prioritizes essential functions under energy constraints [44]. Together, these results advance our understanding of how intrinsic mitochondrial energy deficits reshape neural activity and cognitive outcomes, and underscore the potential of metabolic biomarkers like GDF15 to inform future interventions targeting brain energy metabolism across both rare mitochondrial diseases and more common neurodegenerative conditions.

Methods

Participants

The Mitochondrial Stress, Brain Imaging, and Epigenetics (MiSBIE) study was conducted in Columbia University Irving Medical Center in adherence to the directives outlined by the New York State Psychiatric Institute IRB protocol #7424, ClinicalTrials.gov NCT04831424. From 2018 to 2023, English-speaking adults aged 18–60 were enrolled through clinical and research networks at Columbia University (e.g., the Neuromuscular Clinic, RecruitMe), the Children's Hospital of Philadelphia, and national/international organizations focused on mitochondrial disease (e.g., NAMDC, UMDF). Participants were excluded for recent illness, pregnancy, current cancer, use of steroids, participation in other clinical trials, or cognitive impairment (TICS-41 ≤30). Behavior Participants visited Columbia University Irving Medical Center for two consecutive days of data collection, including biospecimen collection, medical exam, stress reactivity–recovery session, detailed physiological measurements, standing and functional capacity test, metabolic rate analysis, psychosocial questionnaires, and neuropsychological assessment. On the second day, participants visited The Zuckerman Institute at Columbia University for brain imaging, including T1, T2, field map, resting state, Diffusion-Weighted Imaging (DWI), and task fMRI [101].

In total, 110 participants are included in the Mitochondrial Stress, Brain Imaging, and Epigenetics (MISBIE) study. 40 MitoD patients, including 20 patients with m.3243A>G mutation, 15 patients with single deletion in mDNA, and 5 patients with Mitochondrial Encephalomyopathy (MELAS), with 70 healthy controls. The age and gender are matched between the two groups (Figure S5). High-resolution structural and functional MRI data were available for 91 participants (29 MitoD: 16 point mutations, 11 deletions, 2 MELAS; and 62 controls). Because some individuals did not complete every fMRI task or were excluded for poor behavioral performance below 40% or missing behavioral outputs, the final sample sizes differed by task: for the N-back working memory task, 88 participants (28 MitoD: 15 point mutations, 11 deletions, 2 MELAS) provided usable data, of whom 74 (25 MitoD: 14 point mutations, 9 deletions, 2 MELAS) remained after accuracy exclusions; for the cold-pain task, 91 participants (29 MitoD: 16 point mutations, 11 deletions, 2 MELAS) had complete data; and for the multisensory task, 90 participants (28 MitoD: 16 point mutations, 10 deletions, 2 MELAS) were included.

Materials and Procedures

In addition to neuroimaging, all participants completed a comprehensive phenotypic battery covering eleven domains. Self-report questionnaires assessed key psychological factors (anxiety, depression, burnout, stress, personality traits, PTSD symptoms, tic severity), social and environmental exposures (social support, childhood trauma, life events), and health behaviors (physical activity, sleep quality). Clinically relevant symptom scales captured fatigability (physical, cognitive, psychosocial), autonomic dysfunction, and headache severity, while objective tests measured sit-to-stand performance, body composition, pulmonary function (FEV_1, FVC), and neurological status (NMDAS, CNS score, Karnofsky). Cognitive function was probed with standardized neuropsychological tasks of executive control, memory, and fluid intelligence (e.g., verbal fluency, trail-making, Stroop, RBANS, WASI). Resting energy metabolism and respiratory parameters were quantified via indirect calorimetry, and stress reactivity was indexed by heart rate, respiration, and salivary cortisol. Finally, blood and saliva assays provided markers of mitochondrial energetics (mtDNA copy number), metabolic health (glucose, lipids, electrolytes, HbA_1c), mitochondrial stress (GDF15, FGF21, lactate), and immune/inflammatory status (CBC, CRP, fibrinogen). (See [101] for more details)

A comprehensive assessment,including the Newcastle Mitochondrial Disease Adult Scale (NMDAS), Columbia Neurological Score (CNS), Karnofsky Performance Scale (KPS), Composite Autonomic Symptom Score (COMPASS), and Modified Fatigue Impact Scale (MFIS), was administered to capture the multisystem impact of mitochondrial disease. The NMDAS provides a standardized index of disease-specific symptom severity across neuromuscular, exercise intolerance, and metabolic domains. The CNS aggregates clinician-rated neurological findings (e.g., cranial nerve function, coordination, gait, and cognition) into a single severity score. The KPS rates overall functional capacity on a 0–100 scale, reflecting a patient's ability to perform daily activities and self-care. The COMPASS quantifies autonomic dysfunction across orthostatic, vasomotor, sudomotor, gastrointestinal, bladder, and pupillomotor systems, yielding both domain-specific and total autonomic burden scores. Finally, the MFIS assesses the perceived impact of fatigability on physical, cognitive, and psychosocial functioning. Together, these instruments provide a comprehensive clinical profile—ranging from symptom burden and neurological impairment to daily-life functioning and autonomic stability—that we used both to characterize group differences and to relate systemic disease severity to neuroimaging and metabolic biomarkers.

MRI Experimental paradigm

The MRI session for the MISBIE study took place on the second day of the participants' visit. The imaging acquisition followed a sequence that included a localizer (1 minute), a field map (1 minute), a T2 structural scan (11 minutes and 15 seconds), a T1 structural scan (5 minutes and 21 seconds), a multisensory task (5 minutes), a resting state scan (10 minutes and 51 seconds), an N-back task (2 runs, each lasting 4 minutes and 28 seconds), a social-evaluative task (6 minutes), and a cold pain task (6 minutes), ending with a DWI scan (Sequence 1-2, 6 minutes and 27 seconds). In the current analysis, we focused on the resting state and task data from the multisensory, N-back, and cold pain tasks. The speech preparation task was discarded due to misalignment issues between the experiment output and the MRI data.

Multisensory Task (Basic Sensory)

In the multisensory task, participants were exposed to both visual stimulation (a flickering checkerboard pattern) and auditory stimulation (a sequence of sounds with gradually increasing and decreasing pitch) presented in a 30-second block (See settings also in [102]). Each task block was preceded by a 30-second resting block during which participants were instructed to fixate on a central cross. The entire session lasted 6 minutes, with the rest-task cycle repeated three times. The contrast between the task and rest periods was used to model the brain's response to multisensory processing in the fMRI analysis.

N-back Task (Working Memory)

The N-back task followed a block design as described previously [103]. Within each task block, a word was presented for one second to indicate the block type (0-back or 2-back). Each block consisted of 10 trials featuring 10 different stimuli of the same type, and each block used a different set of stimuli. Participants were instructed to respond with a button press, indicating either "yes, this image matches the image presented n trials ago" (target response) or "no, this image does not match the image presented n trials ago" (nontarget response). Responses were recorded to calculate behavioral accuracy. Both the 2-back and 0-back blocks lasted 25 seconds, followed by a 15-second rest period. The contrast between the 2-back (high cognitive load) and 0-back (low cognitive load) conditions was used to model the brain's response during working memory tasks.

Cold Pain Task (Negative Affect)

In the cold pain task, the study coordinator equipped the participant with the MR-compatible Cold Pressor Arm Wrap (CPAW). At the beginning of the session, the coordinator first placed a

room-temperature wrap on the participant's right hand and wrist for 90 seconds. This was followed by a 30-second buffer period before applying the cold pack, which then covered the right hand and wrist for an additional two minutes. After a second 30-second buffer period, the session concluded with a 90-second recovery period using the room-temperature wrap. Inside the cold wrapper, Solution is MRI-safe gelpacs. The coldpack were stored in a small freezer set to approximately 0 °F (though temperatures could vary slightly) and were removed about 15 minutes before the task to reach a safe, near-freezing temperature. The procedure conducted in the experiment is as follows [104] . In the fMRI analysis, the contrast between the cold pressor and the initial room-temperature period was used to model the brain's response to cold pain.

To confirm that the CPAW elicited pain, we had participants rate their discomfort on a 0–10 scale at the end of the experiment (0 = no pain; 10 = intolerable). Nearly all participants reported scores above zero, indicating the stimulus was painful. Mean (± SD) pain ratings were 3.9 ± 2.5 in the control group and 4.2 ± 2.2 in the MitoD group; this difference was not significant ($t = -0.51$, $p = 0.61$, $df = 93$).

Imaging acquisition parameters

In the MRI session, we measured brain anatomy using T1- and T2-weighted magnetic resonance imaging on a 3 T Siemens Prisma scanner (Siemens Medical Solutions). The sequence parameters for T1 were: echo time, 0.00349 s; repetition time, 2.3 s; flip angle, 8°; voxel size, 1 × 1 × 1 mm; slice thickness, 1 mm. Parallel imaging with a reduction factor of 2 was used. The parameters for T2 were: echo time, 0.562 s; repetition time, 3.2 s; flip angle, 120°; voxel size, 0.7 × 0.7 × 0.7 mm; slice thickness, 0.7 mm. Parallel imaging with a reduction factor of 2 was used. We collected functional MRI images on the same scanner to measure BOLD activity during a series of psychological tasks. The sequence parameters were as follows: echo time, 0.029 s; repetition time, 0.46 s; flip angle, 44°; voxel size, 3.02 × 3.02 × 3 mm; slice thickness, 3 mm. Slices were acquired with a multiband acceleration factor of 8.

Data preprocessing

Data is transformed into the standard Brain Imaging Data Structure (BIDS) format and preprocessed by fMRIprep [105].

Anatomical images were processed with fMRIPrep (v20.2.1). T1-weighted volumes were bias-field corrected and skull-stripped. Tissue segmentation into gray matter, white matter, and cerebrospinal fluid was performed, and cortical surfaces were reconstructed. The resulting brain mask and surfaces were used to guide nonlinear normalization of the anatomical volume to the MNI152 template space.

Functional preprocessing was also carried out with fMRIPrep (v20.2.1). For each BOLD run, a reference volume was generated, and head-motion parameters were estimated. Slice-timing correction and motion realignment were applied, then functional data were co-registered to the T1-weighted image. Field-map–based distortion correction was disabled due to mismatched shim parameters between field maps and functional scans. Physiological and motion confounds—including framewise displacement, DVARS, and CompCor components—were computed, and motion outlier frames were flagged. Finally, preprocessed time series were normalized to MNI152 space and projected onto the fsaverage surface for surface-based analyses.

Resting state analysis

After preprocessing by fMRI prep, resting state data is further processed by regressing out nuisance covariate including 24 headmotion parameters extracted from fMRIprep and CSF signal and its derivatives. An additional covariate measurement includes spike indicator regressors that detected outliers based on Mahalanobis distance, which measures how different each image is from the rest of the images. An image is detected as a spike if its corresponding Mahalanobis distance is outside the 95% confidence region of the cloud of images in multidimensional space. Multiple comparison is controlled by $p<0.05$ (Bonferroni). In the regressor, each individual potential outlier was coded as 1, and other volumes were coded as 0. Additionally, the data is detrended and smoothed using a 4mm Gaussian smooth kernel for further analysis.

To calculate the regional connectivity and spontaneous activity across brain, a Regional Homogeneity (Reho) analysis and an Amplitude of Low Frequency Fluctuations (ALFF) are done using Data Processing & Analysis of Brain Imaging (DIPABI) software [106]. Band-pass filter is applied for ALFF in 0.01-0.1Hz and 0.01-0.08Hz for Reho.

Task data analysis

Within-participant task effects were estimated using a general linear model (GLM). Robust regression was applied in the GLM to reduce the influence of outliers and improve sensitivity to the task signal [107]. Task and control blocks were modeled as regressors using boxcar functions convolved with the canonical hemodynamic response function (HRF) via CanlabTools (https://github.com/canlab).

The timing and duration of the regressors of interest were based on the onset and duration of each stimulus. A high-pass filter or detrending was applied to remove low-frequency temporal drift, depending on the task design. Specifically, both high-pass filtering and detrending were applied in the multisensory and N-back tasks. In contrast, only detrending was applied in the cold pain task because the relatively long task blocks could lead to the loss of task-related signals if a high-pass filter were used. Nuisance regressors included 24 head motion parameters (six rigid-body motion parameters, their squares, and their temporal derivatives), spike indicator regressors for potential outliers, and cerebrospinal fluid (CSF) time series along with their derivatives. CSF time series were extracted using CANlab tools from canonical CSF masks. The six head motion covariates were derived from the realignment parameters generated by fMRIPrep. Spike regressors were defined as described in the resting-state analysis section.

For each condition (task and control), whole-brain beta coefficient maps were generated separately at the participant level. At the group level, participants' beta maps were compared between task and control conditions. The contrasts of interest included ‘Cold’ vs. ‘Room Temperature’ in the cold pain task, ‘2-back’ vs. ‘0-back’ in the N-back task, and ‘Multisensory’ vs. ‘Rest’ in the multisensory task. In the second-level analysis, CSF signals were regressed out for each participant to control for potential confounds. The processed data were then used for final analyses.

Machine learning classification

A support vector machine (SVM) was applied to decode whole-brain neural representations between the task and control states (e.g., 2-back vs. 0-back in a working memory task). Decoding was performed at the participant level. Specifically, participant-level beta maps for each condition were used to train the SVM to classify task vs. control conditions using leave-one-participant-out cross-validation. The resulting SVM weight map was computed.

To ensure the stability of the weight map, we conducted 5,000 bootstrap tests, generating a bootstrap distribution that allowed us to evaluate the statistical significance of the weight value in each voxel. Finally, the difference in pattern expression between task and control beta maps was used to index the degree of task engagement for each participant, referred to as ‘task brain expression’.

References

1. Attwell, D. & Laughlin, S. B. An energy budget for signaling in the grey matter of the brain. *J Cereb Blood Flow Metab* **21**, 1133–1145 (2001).
2. Raichle, M. E. & Gusnard, D. A. Appraising the brain's energy budget. *Proc Natl Acad Sci U S A* **99**, 10237–10239 (2002).
3. Padamsey, Z. & Rochefort, N. L. Paying the brain's energy bill. *Curr. Opin. Neurobiol.* **78**, 102668 (2023).
4. Raichle, M. E. Two views of brain function. *Trends Cogn. Sci.* **14**, 180–190 (2010).
5. Sibson, N. R. *et al.* Stoichiometric coupling of brain glucose metabolism and glutamatergic neuronal activity. *Proc Natl Acad Sci U S A* **95**, 316–321 (1998).
6. Dienel, G. A. Brain glucose metabolism: Integration of energetics with function. *Physiol. Rev.* **99**, 949–1045 (2019).
7. Mujica-Parodi, L. R. *et al.* Diet modulates brain network stability, a biomarker for brain aging, in young adults. *Proc. Natl. Acad. Sci. U. S. A.* **117**, 6170–6177 (2020).
8. Imaizumi, T. *et al.* Identifying high-risk population of depression: association between metabolic syndrome and depression using a health checkup and claims database. *Sci. Rep.* **12**, 18577 (2022).
9. Saberi, M. *et al.* The brain selectively allocates energy to functional brain networks under cognitive control. *Sci. Rep.* **14**, 32032 (2024).
10. Harper, D. G. *et al.* Tissue type-specific bioenergetic abnormalities in adults with major depression. *Neuropsychopharmacology* **42**, 876–885 (2017).
11. Song, X. *et al.* Bioenergetics and abnormal functional connectivity in psychotic disorders.

Mol. Psychiatry **26**, 2483–2492 (2021).

12. Khaliulin, I., Hamoudi, W. & Amal, H. The multifaceted role of mitochondria in autism spectrum disorder. *Mol. Psychiatry* **30**, 629–650 (2025).
13. Du, F. *et al.* Abnormalities in high-energy phosphate metabolism in first-episode bipolar disorder measured using 31P-magnetic resonance spectroscopy. *Biol. Psychiatry* **84**, 797–802 (2018).
14. Procaccini, C. *et al.* Role of metabolism in neurodegenerative disorders. *Metabolism* **65**, 1376–1390 (2016).
15. Anandhan, A. *et al.* Metabolic dysfunction in Parkinson's disease: Bioenergetics, redox homeostasis and central carbon metabolism. *Brain Res. Bull.* **133**, 12–30 (2017).
16. Freyberg, Z., Ford, J. M. & Phillips, M. L. Metabolism matters in mental health. *Biol. Psychiatry Cogn. Neurosci. Neuroimaging* **10**, 239–240 (2025).
17. Monzel, A. S., Enríquez, J. A. & Picard, M. Multifaceted mitochondria: moving mitochondrial science beyond function and dysfunction. *Nat. Metab.* **5**, 546–562 (2023).
18. Picard, M. & Shirihai, O. S. Mitochondrial signal transduction. *Cell Metab.* **34**, 1620–1653 (2022).
19. Pekkurnaz, G. & Wang, X. Mitochondrial heterogeneity and homeostasis through the lens of a neuron. *Nat. Metab.* **4**, 802–812 (2022).
20. Mosharov, E. V. *et al.* A human brain map of mitochondrial respiratory capacity and diversity. *Nature* **641**, 749–758 (2025).
21. Castrillon, G. *et al.* An energy costly architecture of neuromodulators for human brain evolution and cognition. *bioRxiv* (2023) doi:10.1101/2023.04.25.538209.
22. Mattson, M. P., Gleichmann, M. & Cheng, A. Mitochondria in neuroplasticity and neurological disorders. *Neuron* **60**, 748–766 (2008).

23. Cline, S. D. Mitochondrial DNA damage and its consequences for mitochondrial gene expression. *Biochim. Biophys. Acta* **1819**, 979–991 (2012).
24. Arrázola, M. S. *et al.* Mitochondria in developmental and adult neurogenesis. *Neurotox. Res.* **36**, 257–267 (2019).
25. Brunetti, D., Dykstra, W., Le, S., Zink, A. & Prigione, A. Mitochondria in neurogenesis: Implications for mitochondrial diseases. *Stem Cells* **39**, 1289–1297 (2021).
26. Rosenberg, A. M. *et al.* Brain mitochondrial diversity and network organization predict anxiety-like behavior in male mice. *Nat. Commun.* **14**, 4726 (2023).
27. Sharpley, M. S. *et al.* Heteroplasmy of mouse mtDNA is genetically unstable and results in altered behavior and cognition. *Cell* **151**, 333–343 (2012).
28. Hollis, F. *et al.* Mitochondrial function in the brain links anxiety with social subordination. *Proc. Natl. Acad. Sci. U. S. A.* **112**, 15486–15491 (2015).
29. Gebara, E. *et al.* Mitofusin-2 in the nucleus accumbens regulates anxiety and depression-like behaviors through mitochondrial and neuronal actions. *Biol. Psychiatry* **89**, 1033–1044 (2021).
30. Chen, T., He, J., Huang, Y. & Zhao, W. The generation of mitochondrial DNA large-scale deletions in human cells. *J. Hum. Genet.* **56**, 689–694 (2011).
31. Gorman, G. S. *et al.* Prevalence of nuclear and mitochondrial DNA mutations related to adult mitochondrial disease. *Ann. Neurol.* **77**, 753–759 (2015).
32. Gorman, G. S. *et al.* Mitochondrial diseases. *Nat. Rev. Dis. Primers* **2**, 16080 (2016).
33. Picard, M. & Murugan, N. J. The Energy Resistance Principle. (2025) doi:10.31219/osf.io/hgnmj_v2.
34. Set, K. K., Sen, K., Huq, A. H. M. & Agarwal, R. Mitochondrial disorders of the nervous system: A review. *Clin. Pediatr. (Phila.)* **58**, 381–394 (2019).

35. Alston, C. L., Rocha, M. C., Lax, N. Z., Turnbull, D. M. & Taylor, R. W. The genetics and pathology of mitochondrial disease. *J. Pathol.* **241**, 236–250 (2017).
36. Moore, H. L., Blain, A. P., Turnbull, D. M. & Gorman, G. S. Systematic review of cognitive deficits in adult mitochondrial disease. *European Journal of Neurology* **27**, 3 (2019).
37. Schmid, M. C. *et al.* Blindsight depends on the lateral geniculate nucleus. *Nature* **466**, 373–377 (2010).
38. Vuilleumier, P., Richardson, M. P., Armony, J. L., Driver, J. & Dolan, R. J. Distant influences of amygdala lesion on visual cortical activation during emotional face processing. *Nat. Neurosci.* **7**, 1271–1278 (2004).
39. Barbey, A. K., Koenigs, M. & Grafman, J. Dorsolateral prefrontal contributions to human working memory. *Cortex* **49**, 1195–1205 (2013).
40. Saneto, R. P., Friedman, S. D. & Shaw, D. W. W. Neuroimaging of mitochondrial disease. *Mitochondrion* **8**, 396–413 (2008).
41. Friedman, S. D., Shaw, D. W. W., Ishak, G., Gropman, A. L. & Saneto, R. P. The use of neuroimaging in the diagnosis of mitochondrial disease. *Dev. Disabil. Res. Rev.* **16**, 129–135 (2010).
42. Gropman, A. L. Neuroimaging in mitochondrial disorders. *Neurotherapeutics* **10**, 273–285 (2013).
43. Huisman, T. A. G. M., Kralik, S. F., Desai, N. K., Serrallach, B. L. & Orman, G. Neuroimaging of primary mitochondrial disorders in children: A review. *J. Neuroimaging* **32**, 191–200 (2022).
44. Picard, M., Kempes, C., Pontzer, H., Ph. ., Behnke, A. & Shaulson, E. D. Energy constraints on human health. (2025) doi:10.31219/osf.io/ne3qg_v1.
45. Yang, X. *et al.* Physical bioenergetics: Energy fluxes, budgets, and constraints in cells.

Proc. Natl. Acad. Sci. U. S. A. **118**, e2026786118 (2021).

46. Bobba-Alves, N., Juster, R.-P. & Picard, M. The energetic cost of allostasis and allostatic load. *Psychoneuroendocrinology* **146**, 105951 (2022).
47. Sturm, G. *et al.* OxPhos defects cause hypermetabolism and reduce lifespan in cells and in patients with mitochondrial diseases. *Commun. Biol.* **6**, 22 (2023).
48. Sercel, A. J. *et al.* Hypermetabolism and energetic constraints in mitochondrial disorders. *Nat. Metab.* **6**, 192–195 (2024).
49. Jamadar, S. D., Behler, A., Deery, H. & Breakspear, M. The metabolic costs of cognition. *Trends Cogn. Sci.* **29**, 541–555 (2025).
50. Miyake, A. *et al.* The unity and diversity of executive functions and their contributions to complex 'Frontal Lobe' tasks: a latent variable analysis. *Cogn. Psychol.* **41**, 49–100 (2000).
51. Conway, A. R. A., Kane, M. J. & Engle, R. W. Working memory capacity and its relation to general intelligence. *Trends Cogn. Sci.* **7**, 547–552 (2003).
52. Hara, Y., Puri, Y. F., Janssen, R., Rapp, W. & Morrison, P. R. Presynaptic mitochondrial morphology in monkey prefrontal cortexcorrelates with working memory and is improved with estrogentreatment. *Proc Natl Acad Sci* **111**, 486–491 (2014).
53. Bruckmaier, M., Tachtsidis, I., Phan, P. & Lavie, N. Attention and capacity limits in perception: A cellular metabolism account. *J. Neurosci.* **40**, 6801–6811 (2020).
54. Flippo, K. H. & Potthoff, M. J. Metabolic messengers: FGF21. *Nat. Metab.* **3**, 309–317 (2021).
55. Patel, S. *et al.* GDF15 provides an endocrine signal of nutritional stress in mice and humans. *Cell Metab.* **29**, 707–718.e8 (2019).
56. Chang, J. Y. *et al.* The role of growth differentiation factor 15 in energy metabolism. *Diabetes Metab. J.* **44**, 363–371 (2020).

57. Sharma, R. *et al.* Circulating markers of NADH-reductive stress correlate with mitochondrial disease severity. *J. Clin. Invest.* **131**, (2021).

58. Yarkoni, T., Poldrack, R. A., Nichols, T. E., Van Essen, D. C. & Wager, T. D. Large-scale automated synthesis of human functional neuroimaging data. *Nat Methods* **8**, 665–670 (2011).

59. Bo, K. *et al.* A systems identification approach using Bayes factors to deconstruct the brain bases of emotion regulation. *Nat. Neurosci.* **27**, 975–987 (2024).

60. Kohoutová, L. *et al.* Individual variability in brain representations of pain. *Nat. Neurosci.* **25**, 749–759 (2022).

61. Kragel, P. A., Koban, L., Barrett, L. F. & Wager, T. D. Representation, pattern information, and brain signatures: From neurons to neuroimaging. *Neuron* **99**, 257–273 (2018).

62. Baranger, D. A. *et al.* Enhancing task fMRI individual difference research with neural signatures. *medRxiv* (2025) doi:10.1101/2025.01.30.25321355.

63. Rouder, J. N., Speckman, P. L., Sun, D., Morey, R. D. & Iverson, G. Bayesian t tests for accepting and rejecting the null hypothesis. *Psychon. Bull. Rev.* **16**, 225–237 (2009).

64. Tomasi, D., Wang, G.-J. & Volkow, N. D. Energetic cost of brain functional connectivity. *Proc. Natl. Acad. Sci. U. S. A.* **110**, 13642–13647 (2013).

65. Godbersen, G. M. *et al.* Task-evoked metabolic demands of the posteromedial default mode network are shaped by dorsal attention and frontoparietal control networks. *Elife* **12**, e84683 (2023).

66. Zou, Q.-H. *et al.* An improved approach to detection of amplitude of low-frequency fluctuation (ALFF) for resting-state fMRI: fractional ALFF. *J. Neurosci. Methods* **172**, 137–141 (2008).

67. Zang, Y., Jiang, T., Lu, Y., He, Y. & Tian, L. Regional homogeneity approach to fMRI data

analysis. *Neuroimage* **22**, 394–400 (2004).

68. Fujita, Y. *et al.* GDF15 is a novel biomarker to evaluate efficacy of pyruvate therapy for mitochondrial diseases. *Mitochondrion* **20**, 34–42 (2015).
69. Huang, Q. *et al.* The energetic stress marker GDF15 is induced by acute psychosocial stress. *bioRxivorg* (2024) doi:10.1101/2024.04.19.590241.
70. Deng, Y.-T. *et al.* Atlas of the plasma proteome in health and disease in 53,026 adults. *Cell* **188**, 253–271.e7 (2025).
71. Huang, Q. *et al.* The mitochondrial disease biomarker GDF15 is dynamic, quantifiable in saliva, and correlates with disease severity. *Mol. Genet. Metab.* **145**, 109179 (2025).
72. Shaulson, E. D., Cohen, A. A. & Picard, M. The brain-body energy conservation model of aging. *Nat. Aging* **4**, 1354–1371 (2024).
73. Tanaka, T. *et al.* Plasma proteomic biomarker signature of age predicts health and life span. *Elife* **9**, e61073 (2020).
74. Lehallier, B. *et al.* Undulating changes in human plasma proteome profiles across the lifespan. *Nat. Med.* **25**, 1843–1850 (2019).
75. Trumpff, C. *et al.* Blood mitochondrial health markers cf-mtDNA and GDF15 in human aging. *Physiology* (2025).
76. Wen, H. *et al.* Mitochondrial diseases: from molecular mechanisms to therapeutic advances. *Signal Transduct. Target. Ther.* **10**, 9 (2025).
77. Turner, N. & Heilbronn, L. K. Is mitochondrial dysfunction a cause of insulin resistance? *Trends Endocrinol. Metab.* **19**, 324–330 (2008).
78. Pappas, C. *et al.* Blood glucose levels may exacerbate executive function deficits in older adults with cognitive impairment. *J. Alzheimers. Dis.* **67**, 81–89 (2019).
79. Rowland, L. *et al.* 12.4 brain lactate is related to cognition in schizophrenia. *Schizophr. Bull.*

44, S20–S21 (2018).

80. Cunnane, S. C. *et al.* Can ketones compensate for deteriorating brain glucose uptake during aging? Implications for the risk and treatment of Alzheimer's disease. *Ann N Y Acad Sci* **1367**, 12–20 (2016).
81. Ross, J. M. *et al.* High brain lactate is a hallmark of aging and caused by a shift in the lactate dehydrogenase A/B ratio. *Proc Natl Acad Sci U S A* **107**, 20087–20092 (2010).
82. Camandola, S. & Mattson, M. P. Brain metabolism in health, aging, and neurodegeneration. *The EMBO Journal* (2017) doi:10.15252/embj.201695810.
83. Ripp, I. *et al.* Working memory task induced neural activation: A simultaneous PET/fMRI study. *Neuroimage* **237**, 118131 (2021).
84. DiNuzzo, M. *et al.* Perception is associated with the brain's metabolic response to sensory stimulation. *Elife* **11**, (2022).
85. Wan, B., Riedl, V., Castrillon, G., Kirschner, M. & Valk, S. L. Bridging Glucose Metabolism and Intrinsic Functional Organization of the Human Cortex. *Neuroscience* (2024).
86. Theriault, J. E. *et al.* A functional account of stimulation-based aerobic glycolysis and its role in interpreting BOLD signal intensity increases in neuroimaging experiments. *Neurosci. Biobehav. Rev.* **153**, 105373 (2023).
87. Raichle, M. E. The brain's dark energy. *Science* **314**, 1249–1250 (2006).
88. Hyder, F., Fulbright, R. K., Shulman, R. G. & Rothman, D. L. Glutamatergic function in the resting awake human brain is supported by uniformly high oxidative energy. *J. Cereb. Blood Flow Metab.* **33**, 339–347 (2013).
89. Anglin MD FRCP(C), R., Garside MD PhD FRCP(C), S., Tarnopolsky MD PhD FRCP(C), M., Mazurek MD FRCP(C), M. & Rosebush MScN MD FRCP(C), P. The psychiatric manifestations of mitochondrial disorders: A case and review of the literature.

Psychiatrist.com (2012).

90. Jou, S.-H., Chiu, N.-Y. & Liu, C.-S. Mitochondrial dysfunction and psychiatric disorders. *Chang Gung Med. J.* **32**, 370–379 (2009).
91. Ochsner, K. N., Silvers, J. A. & Buhle, J. T. Functional imaging studies of emotion regulation: a synthetic review and evolving model of the cognitive control of emotion. *Ann. N. Y. Acad. Sci.* **1251**, E1–24 (2012).
92. Morawetz, C., Bode, S., Derntl, B. & Heekeren, H. R. The effect of strategies, goals and stimulus material on the neural mechanisms of emotion regulation: A meta-analysis of fMRI studies. *Neurosci. Biobehav. Rev.* **72**, 111–128 (2017).
93. Harada, C. N., Natelson Love, M. C. & Triebel, K. L. Normal cognitive aging. *Clin. Geriatr. Med.* **29**, 737–752 (2013).
94. Bernardo, T. C. *et al.* Physical exercise and brain mitochondrial fitness: The possible role against Alzheimer's disease. *Brain Pathol.* **26**, 648–663 (2016).
95. Marseglia, A. *et al.* Metabolic syndrome is associated with poor cognition: A population-based study of 70-year-old adults without dementia. *J. Gerontol. A Biol. Sci. Med. Sci.* **76**, 2275–2283 (2021).
96. Féart, C., Samieri, C. & Barberger-Gateau, P. Mediterranean diet and cognitive function in older adults. *Curr. Opin. Clin. Nutr. Metab. Care* **13**, 14–18 (2010).
97. Maeda, K. *et al.* Clinical phenotype and segregation of mitochondrial 3243A>G mutation in 2 pairs of monozygotic twins. *JAMA Neurol.* **73**, 990 (2016).
98. Picard, M. & Hirano, M. Disentangling (epi)genetic and environmental contributions to the mitochondrial 3243A>G mutation phenotype: Phenotypic Destiny in mitochondrial disease? *JAMA Neurol.* **73**, 923–925 (2016).
99. Jain, I. H. *et al.* Hypoxia as a therapy for mitochondrial disease. *Science* **352**, 54–61

(2016).

100. Kelly, C. *et al.* Perceived association of mood and symptom severity in adults with mitochondrial diseases. *Mitochondrion* **84**, 102033 (2025).

101. Kelly, C. *et al.* A platform to map the mind-mitochondria connection and the hallmarks of psychobiology: the MiSBIE study. *Trends Endocrinol. Metab.* **35**, 884–901 (2024).

102. López-Solà, M. *et al.* Towards a neurophysiological signature for fibromyalgia. *PAIN* **158**, 34 (2017).

103. Barch, D. M. *et al.* Function in the human connectome: task-fMRI and individual differences in behavior. *Neuroimage* **80**, 169–189 (2013).

104. Porcelli, A. J. An alternative to the traditional cold pressor test: The cold pressor arm wrap. *J. Vis. Exp.* (2014) doi:10.3791/50849-v.

105. Esteban, O. *et al.* fMRIPrep: a robust preprocessing pipeline for functional MRI. *Nat Methods* **16**, 111–116 (2019).

106. Yan, C. G., Wang, X. D., Zuo, X. N. & Zang, Y. F. DPABI: Data Processing & Analysis for (Resting-State) Brain Imaging. *Neuroinformatics* **14**, (2016).

107. Wager, T. D., Keller, M. C., Lacey, S. C. & Jonides, J. Increased sensitivity in neuroimaging analyses using robust regression. *Neuroimage* **26**, 99–113 (2005).

Acknowledgements

This work was supported by the National Institutes of Health under grants RF1AG076821, R01MH137190, R37MH076136,R21MH113011, and R01MH122706; the Seed Grant Program for MR Studies of the Zuckerman Mind Brain Behavior Institute at Columbia University; the Robert N. Butler Columbia Aging Center Fellowship Program at the Mailman School of Public Health; the National Center for Advancing Translational Sciences (UL1TR001873) and the

National Cancer Institute (P30CA013696); the Columbia Irving Institute Scholars Program; the Wharton Fund; and the Baszucki Group (to M.P.).

Matlab code for analyses is available at: https://github.com/canlab, with documentation and examples at https://canlab.github.io. Additional information about the MiSBIE study are available at www.picardlab.org/MiSBIE

Supplementary figures

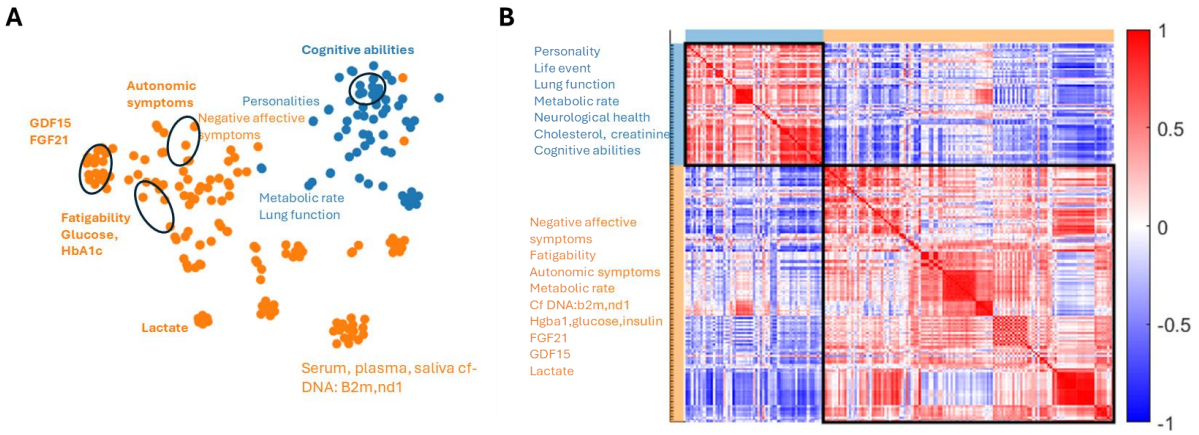

Figure S1 MitoD-specific relationship between measurements in the Phenome. **A)**t-SNE visualization of all measurements, with clusters defined by hierarchical clustering and color-coded accordingly. Measurements that remain significant after FDR correction ($q < 0.05$) are circled and bolded. **B)** Correlation matrix of all measurements using spearman correlation, with hierarchical clustering used to sort the variables. Red and blue indicate positive and negative correlations, respectively, highlighting distinct phenotypic clusters and cross-domain associations.

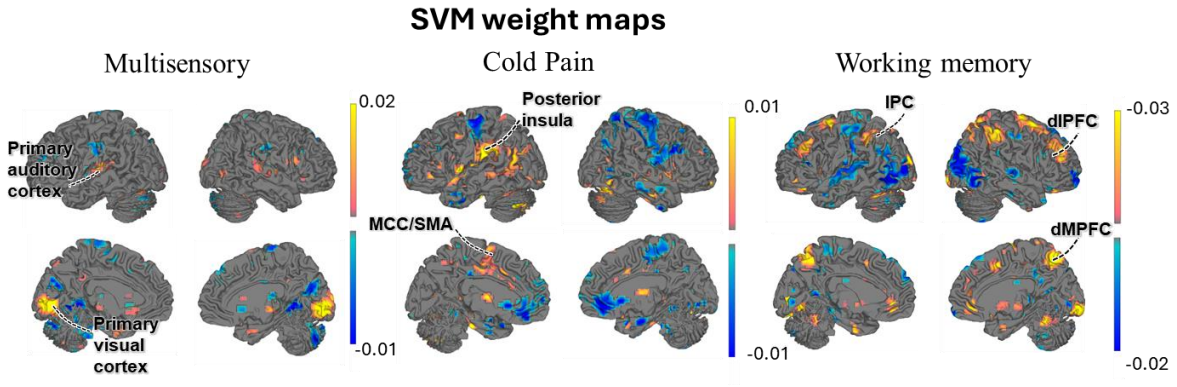

Figure S2 $p < 0.05$ uncorrected SVM weight maps for each task.

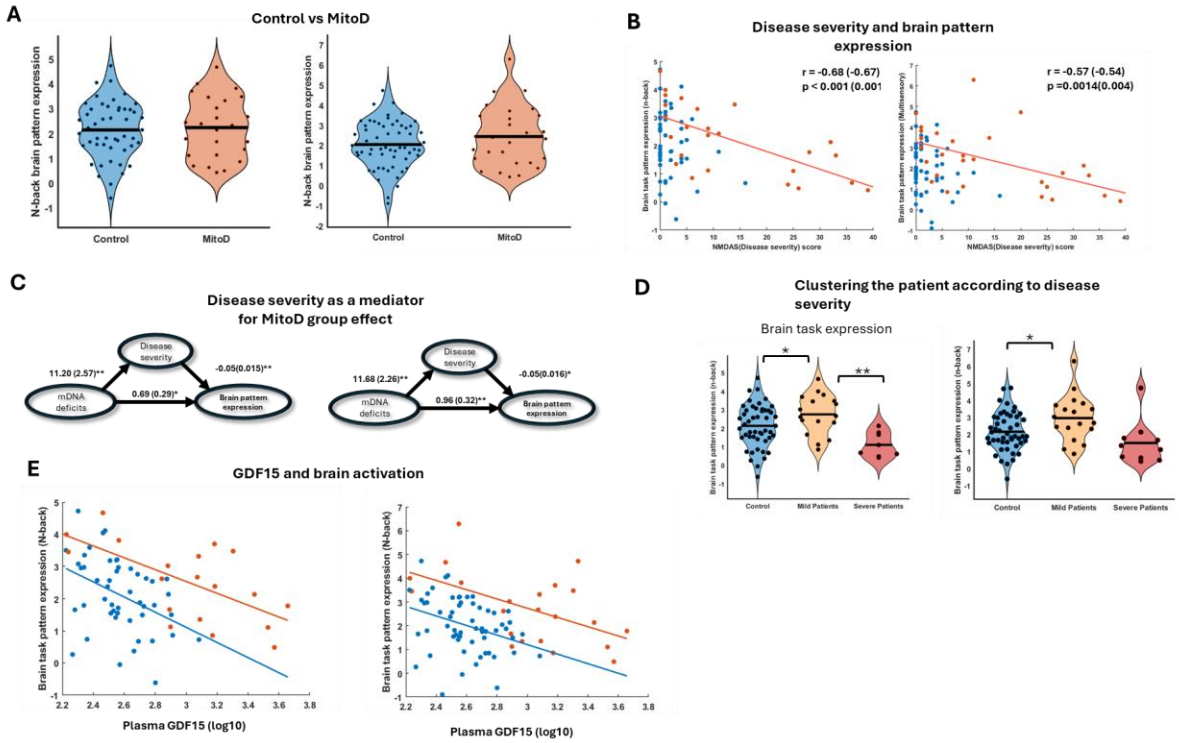

Figure S3. Equivalent tests for all analysis figures involving brain pattern expression after exclusion of participants that have abnormal behavioral performance (Left), versus before exclusion (Right). A) Analysis for figure 3C. B) Analysis for figure 4B. C) Analysis for figure 4C. D) Analysis for figure 4D. E. Analysis for figure 6B. All statistical inference stays the same except for figure 4D, where we don't see significant difference between newly grouped Severe and Mild patients.

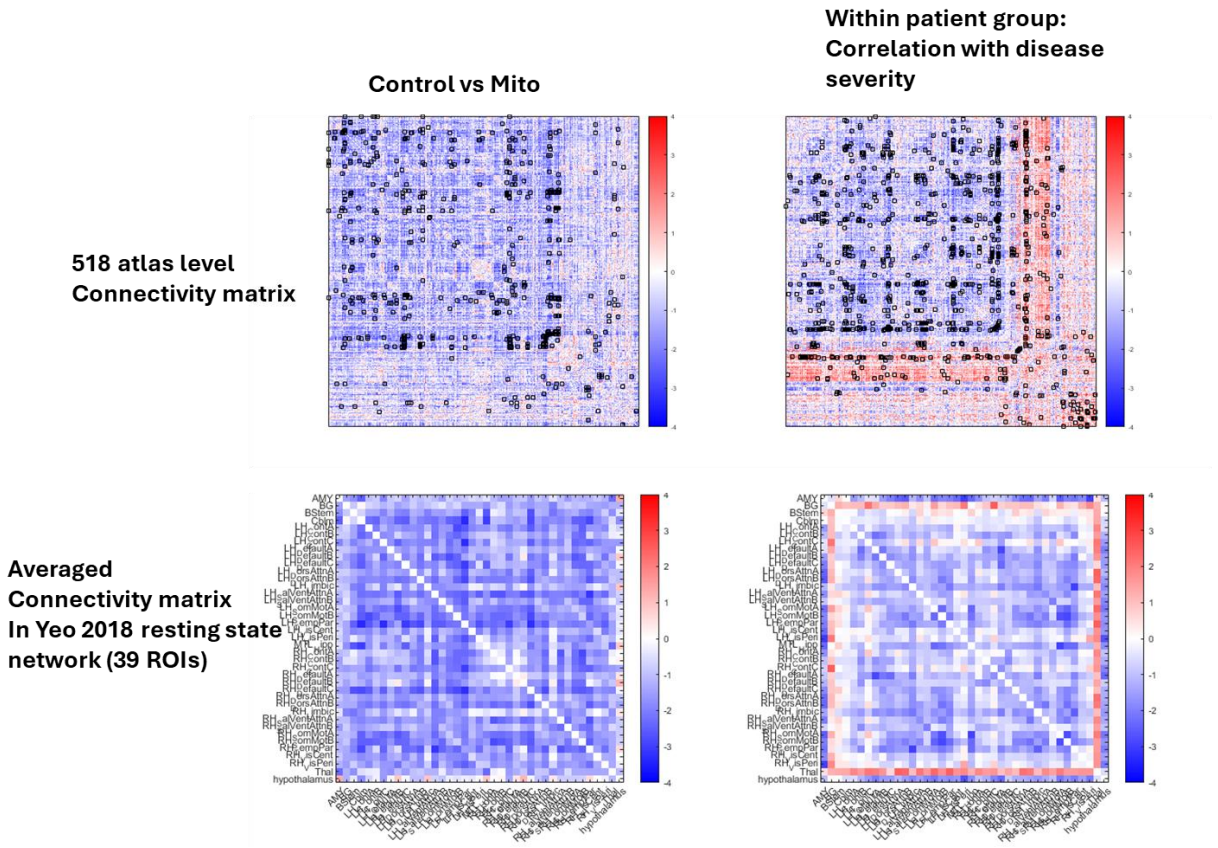

Figure S4. Resting-state fMRI analyses reveal limited group-level effects in atlas-level and more fine-grained network-level. **A)** Functional connectivity analysis across 518 atlas defined from canlab2024 atlas (https://canlab.github.io/_pages/using_canlab_atlases/using_canlab_atlases.html). Group-level connectivity matrices (right) show between-network connectivity for controls vs MitoD (left) and associations with disease severity (right). No results can survive from FDR correction. Effect that has $p<0.001$ has shown using black contour. **B)** Results from A) is averaged within resting-state network from Yeo et al.,2018. No results can survive from FDR correction $q < 0.05$ or $p < 0.001$.

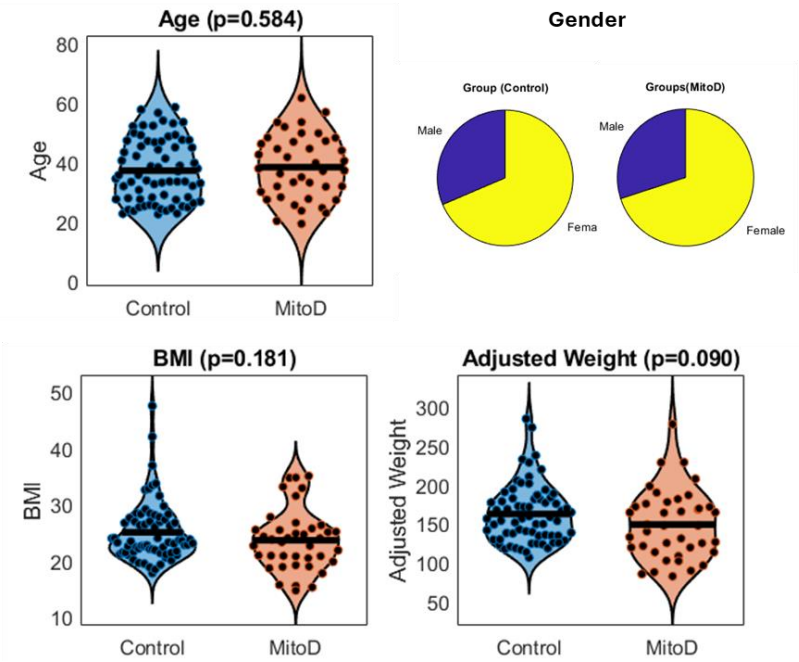

Figure S5 Demographics and anthropometrics information by group. Violin plots compare age, BMI, and adjusted weight between control and MitoD participants. Pie charts depict the sex distribution—percentage of males and females—in each group.